WIS-95/31/July-PH

CsI UV photocathodes: history and mystery

A. Breskin
Department of Particle Physics
The Weizmann Institute of Science
76100 Rehovot, Israel.

Abstract

CsI films are known to be efficient photoconvertors, intensively investigated for UV-photon imaging devices. The article reviews the production and characterization techniques of CsI photocathodes and their photoemission properties in vacuum and gas media, in charge collection and multiplication modes. The important roles of surface phenomena, gas and electric fields are described. The stability of the films is discussed

To be published in Nuclear Instruments and Methods in Physics Research A

Invited talk at the 2nd Int. Workshop on RICH Counters Uppsala, Sweden, 12-16 June, 1995

1. Introduction

Though known for a few decades [1,2], CsI photoconvertors have attracted considerable interest in recent years. Combined with vacuum or gaseous electron multipliers, these photocathodes provide an efficient means for UV-photon imaging over a considerable spectral range [3]. It is limited in the short wavelengths by optical window or gas absorption and reaches a cutoff in the long wavelengths around 210 nm ($E_g \cong 6$ eV). Out of a series of alkali halides, CsI has the largest quantum efficiency (QE)[2] (see Fig.1). This is due, on the one hand, to its low electron affinity (E_a = 0.1-0.2 eV) and on the other hand to its exceptionally large electron escape length, of the order of 16 nm for 1 eV electrons [4] (see Fig. 2). The latter is due to an efficient electron transport mechanism, dominated by electron-phonon interactions, characterized by very small energy losses between collisions. Indeed, the QE of CsI surpasses that of all known solid UV-photocathodes [5]. It is comparable to that of TMAE [tetrakis (dimethylamine) ethylene] vapours [6] in the short wavelengths but is smaller by about a factor of two above 190 nm. On the other hand, compared to gas photoconversion, affecting the time response, occupancy and localization properties of the photodetector, CsI-based devices have the advantage of surface conversion and emission. The latter is of prime importance for operation at very high photon flux and for ultimate localization and timing, even under angular photon incidence. This, and the excellent radiation-induced secondary electron emission properties of CsI, make it a convertor of choice in a novel class of X-ray and thermal neutron imaging detectors [7].

CsI films are simple to prepare and are rather stable when exposed to ambient air. A low sensitivity to exposure to oxygen is indeed expected, for materials having $E_g + E_a >$ 6 eV [8]. This makes CsI photocathodes attractive for use in radiation detectors. Their relatively low volume resistivity, of the order of 10^{10} - 10^{11} $\Omega \cdot$ cm[9], makes possible their stable operation at high radiation fluxes, under high multiplication conditions. Their radiation hardness [10] is important for long term operation at high radiation intensity environments.

There have been several works describing the successful operation of CsI photocathodes in vacuum devices, MCPs and others, mostly in apparatus for space science

[2,3,11,12,13,14]. The detectors incorporated semi-transparent, reflective and even mesh-based CsI photocathodes. It is interesting to note that the latter provided QE values lower by a factor of two, compared to reflective photocathodes, but higher by a factor of two, compared to semi transparent photocathodes [3]. In the case of MCPs, repelling grids in front of the CsI-coated MCP [12,13], enhanced the detection efficiency. The early works on vacuum-based devices discuss the effect of CsI damage after exposure to humid air [15,14,13]. Except for the QE data of Carruthers [3], (i.e. QE (170 nm) $\equiv$ 30%, see Fig. 3) that coincide with present results, as will be discussed in detail below, most ancient works conclude with QE (170 nm) $\approx$ 10%. Part of it is due to the geometrical structure of the MCPs employed.

The idea of mesh-based CsI photocathodes [3] was followed by Ypsilantis in combination with a gaseous multiplier [16], for UV-photon imaging with Ring Imaging Cherenkov (RICH) detectors. This unpublished idea was abandoned because of the venue of TMAE [17]. The idea to replace TEA vapour by a CsI photocathode coupled to a needle gaseous detector for RICH, was suggested by Comby et al. [18,19]. The very low QE values measured by these authors in 1 atm of CH_4, made them abandon this idea.

The revival of CsI-based wire chambers occurred in the late eighties by a few groups, studying independently the possibility of detecting scintillation from Xe [20] and solid scintillators [21], and UV-photons in RICH [22]. The high QE values reported in [22] for CsI and TMAE-coated CsI films, in CH_4, very similar to Carruther's early vacuum data [3], confirmed by other authors [23], and the demonstration of stable operation of CsI-based gaseous photomultipliers under high gain [20,24,25], have no doubt triggered considerable interest in the detector physics community developing RICH devices.

Several groups have launched intensive research work in this field, studying the physical properties of CsI photocathodes and their possible use in gaseous UV detectors particularly for RICH devices [26]. In the course of these studies many contradictory results, mostly on the QE of CsI, were published. Most of the inconsistencies have been clarified, due to a better understanding of the thin film preparation and characterization

procedures, surface phenomena, effects of electric fields, emission into gas media etc. However, some "mysteries" still persist, as will be discussed below. The principal results on the physical properties of CsI photocathodes will be summarized in this article. More complete information and references to other works can be found in the proceedings of the RICH 93 (Bari) [27] and RICH 95 (Uppsala) Workshops.

2. Preparation of thin CsI films

Most of the works deal with relatively thick (a few hundreds of nanometers) CsI films deposited on metal substrates. Thin semitransparent photocathodes (a few tens of nanometers) are usually deposited on optically transparent substrates, coated with very thin metal films [28].

2.1 Film Deposition

The films are usually prepared by resistive vacuum deposition, the substrates being kept at room temperature or heated to 40° - 60°C, as will be discussed below. The evaporation rate is in general of the order of 1-10 nm/s. No significant differences in the QE have been reported for vacuum conditions varying between 10^{-5} - 10^{-8} Torr. However, it is recommended to increase the evaporation rate at worse vacuum conditions, to reduce contamination. The CsI is often deposited on thin Al films (100 nm) coating the substrate metal, usually stainless steel. This procedure should in principle improve the surface quality of the substrate. However, several authors deposit CsI directly on metal substrates. Cu substrates should be avoided because CsI chemically interacts with Cu, seriously degrading the surface quality and the emission properties of the photocathode [29]. Best results, similar to those with stainless steel, with Cu-based printed board pad-electrodes were obtained when coating them with Ni or Ni/Au [30] and Sn/Pb [31], as discussed below.

It was found that the raw CsI material plays some role on the photoemission properties of the photocathode, probably due to the concentration of impurities. In general, most authors use CsI from various origins in a powder of a very thin crystalline form. Anderson et al. [32] reported on a significantly superior QE values, starting from large CsI crystals. Such strong effect has not been observed by others [33] employing

crystals from the same origin (Merck) (see Fig. 4).

The authors of [34] employ electron beam evaporation, claiming for superior surface homogeneity, compared to the usual thermal vacuum deposition. They report on higher QE values of their photocathodes but consider them still as preliminary [35].

Anderson et al. [32] have proposed to spray CsI from a liquid suspension directly on the electrode substrates. This technique could be of interest for very large area devices. However, the relatively good photoemission properties of such films reported by these authors (see Fig. 4a) has not been reproduced so far by other groups.

Porous (low density) CsI films have been investigated [10,36] because of previous experience of an enhanced particle-induced electron emission [37]. Such films are prepared by resistive evaporation under very low Ar pressure.

2.2 Post treatment

The QE of the CsI photocathode is in general low, after the evaporation process. This could result from surface impurities or moisture originating from the substrate material or from the evaporation vessel. Seguinot et al. found that flushing the photocathode surface with pure CH_4, considerably enhances its photoemission properties [22], probably due to the removal of the contaminants (see Fig.5). The enhancement process in this work reached saturation within about 40 h. A faster enhancement, by flushing CH_4 for 4 h, was reported by Anderson et al. [38]; a saturation after about 6 h was also reported by Imrie et al. [39], for CsI on Al and with Ar flush. No enhancement of the photoemission was found by Brauning et al. [40] with CsI deposited on electropolished stainless steel, after flushing with CH_4, at 30 l/h for more than 80 h. Except for Sn/Pb-coated substrates, for which a 40 h flushing yielded some enhancement [31], no effect has been observed by Krizan et al. with other substrate materials. This suggests that the level of surface contamination could be substrate dependent.

A more elegant photoemission enhancement technique was proposed by Anderson et al. [38], consisting of heating the photocathode under gas flow to about 100°C (see Fig. 6). An enhancement effect was found while heating above 40°C under high vacuum [23,40], following the photocathode preparation. The temperature enhancement is considerably faster compared to gas flushing. It should be noted that the experimental

setup of Seguinot et al. has been constantly kept under a temperature of 40°C, which could have also affected their QE enhancement under gas flushing, discussed above.

It has become a routine technique in many laboratories, to also recover the properties of humidity-aged [40] and photon- and ion-aged [23,41] CsI films. It is interesting to note that in the latter the enhancement effect disappears after the temperature decrease. On the other hand, the effect remains very stable when heating the photocathode to 60°C for a few hours in high vacuum, immediately after its deposition on a substrate kept at room temperature or on a hot one [42] (see Fig. 7). There is no significant enhancement of the QE in high vacuum, at room temperature (Fig. 7b). An exception is the lack of temperature enhancement of CsI photocathodes, or rather a deterioration, reported in [41], which could originate from an outgassing process from the Al substrate employed, known for its porosity. However these authors confirm the temperature-induced recovery of humidity-damaged films.

As discussed below, it was found that heat-enhanced CsI films are more stable when exposed to humid air [30]. The post-evaporation enhancement under high vacuum was found to be very successful not only on small samples. It was recently demonstrated that large area (300 x 300 mm^2) heat-enhanced pad photocathodes for RICH have considerably superior photoemission and air-stability properties [30,26,43].

The exact reasons for the heat-enhancement are not yet fully understood and are subject to intensive investigations. We believe that it could have as an origin some chemical, structural and electrical modifications of the CsI surface [83].

3. Microanalysis surface studies

In parallel to standard methods of characterization of CsI photocathode, namely measurements of UV-induced photoemission in a DC mode or in a pulse mode under gas multiplication, important investigations have been carried on in some laboratories to understand the surface properties of the films. The basic idea has been to try and correlate surface effects and morphology to the mode of preparation and to the quantum response of the film.

The most significant work in this field has been done by Coluzza et al. [44]. Several experimental techniques are employed by this group, most important being a laterally

resolved electron spectroscopy for chemical analysis (ESCA) and photoemission electron emission microscopy (PEEM), which permit to correlate photoemission with I or Cs species at the surface. Other complementary techniques like SEM, STM provide the gross structure of the surface. More recent AFM measurements resolve even the atomic structure of CsI, indicating that the polycrystalline surface has indeed a very regular structure that of CsI crystal [30] (see Fig. 8). X-ray diffraction studies provide a good way for studying the chemical composition of the surface, and confirm the crystalline CsI structure [44].

The most significant revelations of the microanalysis studies of thin CsI films are the confirmation of the role of the substrate material on the photoemission yield and the nonhomogeneity of the photoemission correlated with the chemical composition, on a micrometer scale.

It has been demonstrated that very regular polycrystalline structures are contained on inert substrates, with a grain size varying from a fraction of a micron to a few microns, depending on the substrate surface quality. The latter could be modified for example by vacuum coating of the sample metal surface with thin Al or C films; the grain size and the depth of the channels between grains diminishing at larger film thickness [30] (Fig. 9). We still do not know the role of the grain size on the QE, but it could well be that it plays a role on the surface resistivity of the film. Films deposited on Cu substrates present very strong surface nonhomogeneity, reflected by cracks and very irregular crystalline structures [30,44] (Fig. 10). This is due to a chemical reaction between CsI and Cu, followed by surface decomposition into Cs and I species [44]. Thin Au coating of the Cu surface does not prevent this chemical reaction, while thicker Ni, Ni/Au and Sn/Pb coatings of Cu provide very smooth CsI films [30,44]. These substrates, important for the preparation of pad readout electrodes for UV detectors, have very homogenous photoemission properties, compared to that of Cu, as reflected by recent VUV-ESCA studies [44] (see Fig. 11). The superior QE properties of these substrates have been recently confirmed by measurements of photoelectron yields with RICH prototypes [26,31,43].

Laterally resolved UV and X-ray induced photoemission and secondary electron emission studies indicate that on a microscopic scale (3-30 μm) the emission from CsI films

is highly nonhomogeneous. This is true not only for Cu but also for other substrates investigated [44]. The local variations reach factors up to 2-3 and are correlated with the chemical composition of the irradiated area. The enhanced emission is usually correlated with an excess of I atoms.

It should be noted that further microanalysis surface studies could possibly decipher the mystery of the temperature enhancement of photoemission.

4. Quantum efficiency measurements

The quantum efficiency measurements of CsI films have been carried out by several authors in vacuum and gas media. The studies are usually made in three different modes:

a) measuring a DC photocurrent in vacuum or gas under relatively low electric fields.

b) counting pulses in CsI-based wire chambers, under gas multiplication at moderate-to-high fields.

c) counting particle-induced photoelectrons in a CsI-based UV detector in a RICH device.

In a) and b) calibrated monochromatic light sources are used (see for example [22,40,10]), while in c), the quantum efficiency is calibrated against the expected UV photon yield from a known Cherenkov radiator (see for example [45,31].

4.1 Photon flux calibrations

a) TMAE cell

The absolute value of the QE of CsI films is a direct function of the method of calibration of the impinging photon flux. This has been so far the major source of error and discrepancies in QE measurements. Most problematic is the choice of the calibrated reference photosensor.

Seguinot et al. [22] were the first in this field to calibrate the light flux with a TMAE-based photo-ionization cell, relying on the quantum efficiency of TMAE and on photo-absorption measurements in the TMAE vapour. The TMAE cell method has been employed by several groups [40,10,28], but comparisons to other reference photodetectors often provided some discrepancies. We suppose today that such discrepancies could result from systematic errors due to the purity of TMAE, of which

strongly depends the photo-absorption length [46], and the quantum efficiency. Fig. 12 shows indeed considerable differences in the extinction coefficient of TMAE, proportional to the QE, measured by various authors. Some errors would also originate from partial photon absorption by adsorbed TMAE vapours on the windows and electrodes of the TMAE cell. Recent measurements indicate that indeed the problem persists and no good explanation can be provided so far [47].

b) Photomultipliers

Vacuum photomultipliers could be more reliable reference devices, and certainly simpler in routine use, provided they have been calibrated in a correct way. To avoid gain calibration errors, the devices should be operated preferably in a photodiode mode, namely reading the photocurrent from the photocathode with a small positive bias on the first dynode [40]. Their absolute QE values, provided by the suppliers, are usually established against some secondary reference photodetectors, calibrated by National Institutes of Standards. However, probably due to systematic errors in the calibration procedure, some very large errors in the absolute QE values of some photomultiplier tubes have been found [48,49]. The authors of ref. [49] found underestimations in the QE calibration of Hamamatsu R1460 solar blind PM tubes, reaching factors of 2.5, in the wavelength range of 150 - 200 nm (see Fig. 13). The tubes were measured against a fresh NIST-calibrated UV vacuum photodiode (Ball Aerospace Ser. No. 1-926), having a CsTe photocathode. The company admitted having found errors in the calibration procedure. The recalibration of these reference photomultipliers, removed some serious discrepancies in the QE values of CsI films previously reported by the Weizmann Institute and Ecole Polytechique groups [24,40,10,33]. Recent QE measurements of CsI, employing the same type of NIST photodiode, support its validity and superiority as a UV photon calibration standard. Other techniques of photomultiplier calibration are discussed elsewhere [50]. The use of solid state photodiodes as reference photodetectors is limited, because of their small size and inherently large dark current.

4.2 QE measuring techniques

4.2.1 photocurrent in a DC mode

Measuring the UV-induced photocurrent in a DC mode, with reference to a calibrated

photodetector, is the most common and simple technique. Comparative measurements can be made in the same setup, both in vacuum and in gas media. In most laboratories the samples are prepared in one setup and transferred, with a limited contact to air, to another measuring setup. The Weizmann Institute group built a setup that allows to prepare and characterize the films in the same vessel without any exposure to air. Most groups can vary the sample temperature in the measuring setup. Typically, monochromators are used, in vacuum or under inert gas flow, usually equipped with low intensity D_2 lamps (peak at 160 nm). The UV-induced photocurrent from CsI photocathodes under these conditions is usually of 1-100 pA/cm^2.

The bias on the photocathode, in this charge collection mode, is set on the so-called collectors plateau. The plateau in a gas is rather flat at relatively low electric fields, but increases at high fields, under gas multiplication, as discussed below. We will also discuss the dependance of the photoyield on the nature of the gas.

4.2.2 Pulse mode operation

Another way of measuring the quantum efficiency of the photocathode, in gas media, is to count the yield of UV-induced single photoelectron pulses, induced in a CsI-based wire chamber under a known photon flux. Here, lower photon flux are employed, compared to the DC mode. The method also relies on a sound knowledge of the single electron counting efficiency of the detector under study. While some authors compare the photoelectron yield in the same detector filled with TMAE or TEA vapours or operated only with CsI [51,23,54], others compare the wire chamber output with the yield measured with a reference photomultiplier [31,36].

The pulse counting technique simulates real operation conditions of a CsI-based counter, but it does it at very low photon flux and with some uncertainties on the single electron efficiency. The electric field value at the photocathode surface depends on the detector geometry; it is high in a parallel plate geometry, and considerably lower in a multiwire chamber.

As it was recently demonstrated, the electric field strength affects to a large extent the photo-emission [52,53] (see paragraph 5), which could be the origin for some of the discrepancies on the value of the QE of CsI, measured in different modes.

4.2.3 Photo-electron counting in RICH

The QE of CsI can be directly deduced when counting the mean number of photo-electrons per Cherenkov ring in a RICH setup [55,56]. Here again, the counted number of photo-electrons depends on one hand on the single electron detection efficiency and on the other hand, on the efficiency to resolve neighbouring photo-electrons. The latter depends on the pad size of the readout electrode and on the ring diameter. Most important is to take good account of possible photon feedback effects [26,43]. Very systematic and elaborated measurements were done in this field, in a RICH device with an atmospheric pressure wire chamber, by Piuz et al. [56,45,26]. Due to the high chromaticity of the NaF Cherenkov radiator, and the high single photon localization accuracy, these authors could evaluate with good precision the differential QE of CsI. The refractive index of NaF being dependent on the photon energy, a measure of the distance of the photon from the ring centre determines this energy [45]. A similar technique has also been applied by other groups [57,58]. Using this technique one should have a sound knowledge of some other parameters of the RICH device, such as transmission of electrodes, optical windows and the Cherenkov radiator. Recent data of the QE of CsI measured with this technique are very close to those obtained in the DC and pulse counting modes [43,26] (see Fig. 14).

It should be noted here that another method for measuring the QE of CsI, using the Cherenkov effect was proposed [59]. It is based on measuring pulse height distributions of photo-electrons induced in a CsI-based wire chamber by β-particles traversing a NaF radiator. The QE is deduced from comparisons with single electron spectra.

4.3 Summary of QE data of CsI

The QE of CsI has been measured by a very large number of groups. It is interesting to note that in the last two years, after a series of very contradictory published results, most data are in reasonable agreement. The most significant QE results, in our opinion, are presented in table 1.

The table provides information on the measuring technique, the light flux calibration method, the photocathode substrate, and post-evaporation treatment. For reason of

commodity, the QE data are compared at 170 nm; in cases where data were measured at other wavelengths, an extrapolation was made (see data in brackets).

It is interesting to note that most QE data show an average of 25-30% at 170 nm, similar to the early results of Carruthers [3] (see Fig. 3). An exception, 10% at 170 nm [13], is due to geometrical factors of the photocathode, deposited directly on a MCP. Not shown are the somewhat higher results reported in [34], not yet confirmed [35].

It is a very encouraging fact that some recent RICH QE results are very close to those measured on small samples, under optimal laboratory conditions. It should be remembered that in RICH, the CsI is deposited on printed board circuits, whose nature seems to play an important role on the QE (see 2.1, 3). The latter, the emission into gas and the electric field strength could explain some lower QE results obtained so far by some groups in RICH tests. Some QE spectra of different groups are shown in Figs. 15,16,17.

5. Photoemission dependance on the gas and electric field

5.1 Emission into vacuum

Photoemission into vacuum reaches full efficiency at very low electric fields, of the order of a few tens of V/cm. Measurements should be performed in good vacuum conditions (below 10^{-3} Torr), to avoid possible effects of some minor multiplication due to residual gas molecules. Such effects have been indeed observed by us.To avoid possible electron losses due to electric field distortions, the photocurrent should be preferably measured at the photocathode.

At low electric field values the photocurrent reaches a plateau. Some authors have remarked that this plateau has a small slope; the photocurrent increase with the electric field reaches a few percent at fields of a few kV/cm [10,60].

Some authors have observed an enhancement of the photoyield following a discharge at the photocathode surface [52] or under high photon flux [10,45,51]. The enhancement is generally unstable and some authors, who measured the effect under gas amplification, attributed it to a surface modification due to positive ion adsorption [51].

We suggested the enhancement is due to strong local modifications of the electric field due to a slow neutralization of positive ions at the insulator surface [53]. This can result

in the creation of fields reaching several hundreds of kV/cm. According to our model, confirmed by experimental results, the field enhancement of the photo-emission is due to a decrease of the electron work function, similar to the Schottky effect in metals [53].

Systematic measurements of the QE enhancement of CsI under very high electric fields, reaching 500 kV/cm, were done in vacuum, with a multiwire electrode structure shown in Fig. 18. CsI was deposited on 10 μm diameter cathode wires; the high fields could be reached when applying a few kV to the anodes.

The relative enhancement of photoemission from CsI as function of the field is shown in Fig. 19. The wires were illuminated by UV-photon from a source or from Gamma-irradiated BaF_2 and $KMgF_3$ scintillators [52]. One can observe a strong dependence on the wavelength. The enhancement factor of photoemission, under 500 kV/cm at the photocathode surface, is of 1.5 at 160 nm, 3 at 185 nm and 25 above 200 nm. It was measured both on fresh and aged photocathodes. The larger effect at long wavelengths is due to the stronger impact of the affinity reduction on lower energy photoelectrons. Detailed account of the model interpretation is given in [53].

It should be noted that at more moderate electric fields, of the order of 10 kV/cm, the enhancement in photoemission is of 10-20% at 185 nm. This is in agreement with recent observations of other authors [60].

The considerable field enhanced photoemission in vacuum could have some practical impact in photodetectors employing CsI or other photocathodes [42].

5.2 Emission into gas

Photoemission into gas is affected by elastic backscattering of photoelectrons on the gas molecules. This effect is known to be larger in noble gases, due to dominant elastic collisions at low electron energies [61,62,63,64].

The dependence of photoemission on the gas filling has been observed by many authors [24,23,65,66,67]. Best results have always been observed in CH_4, also employed by Seguinot et al., in their early work [22]. Anderson et al. [23] reported on a higher photoemission in CH_4, compared to vacuum, attributing this effect to some CsI surface modifications due to adsorption of CH_4 molecules. We believe today that vacuum

photoemission is always superior to that into gas, and that these observations, also confirmed by others [40], have as an origin some systematic errors in the measurement procedure.

Some recent works treat the emission in gas and its dependence on the electric field in a more systematic way [52,68,69]. In these works, a setup was prepared which permits to study UV-induced photoemission as function of the field, both in collection and charge multiplication modes. The results, obtained in a pulse counting mode, can be compared to that measured in vacuum in a DC mode in the same setup, without exposure to air [52,68].

The emission into a few hydrocarbons has been investigated: CH_4, C_2H_6 and i-C_4H_{10}, into some of their mixtures and into Ar or He mixtures with hydrocarbons. The measurements were carried out at low and atmospheric pressure.

It was found that the photoelectron extraction from solid photocathodes into gas media has a universal behaviour as a function of field. In a charge collection mode, the quantum yield (QY) is always lower than that in vacuum, as also confirmed by Lu et al. [41], and after a rise is independent of the field. In a charge multiplication mode, the QY increases with the field and reaches the vacuum value at high gas gains. The most pronounced behaviour, leading to a very large difference in the QY between the collection and multiplication modes, was observed in He-based gas mixtures (Fig. 20a), also observed in [23,41], while a reduction in the QY observed in Ar-hydrocarbon mixtures approaches that in pure hydrocarbons. In pure CH_4 and some CH_4-hydrocarbon gas mixtures the QY is practically independent of the field and is close to that in vacuum even at low fields and at atmospheric pressure (Fig. 20b). Fig 21 summarizes some of the results of the relative photoemission yield into CH_4 and some He-and Ar-based mixtures.

These results are explained by the difference in extraction efficiency of photoelectrons from CsI, which depends on the elastic backscattering probability from different gas molecules. At high gas gain elastic backscattering is taken over by inelastic collisions, resulting in a QY value equal to that in a vacuum, independently of the gas nature. A detailed discussion of the backscattering effect and results of model calculations, confirming the experimental findings, are given in [69]. It should be noted that the experimental results of photoemission into various gases have been confirmed in a RICH setup with a CsI photocathode coupled to an atmospheric pressure MWPC [43,68,69].

Though CH_4 and CH_4-based hydrocarbon mixtures are best candidates from the point of view of photoemission, safety regulations imply the use of less flammable mixtures. The gas studies [68,69] reflect that Ar/CH_4 (50/50, 80/50) or Ar/i-C_4H_{10} (80/20) mixtures could be good candidates. However, one should be aware of the fact that such mixtures could have larger photon feedback effects at high multiplication factors [43]. These effects and their impact on the detector resolution should be studied in detail.

In addition, the restriction on the gas filling, due to backscattering, applies to detector geometries where the field at the cathode surface is relatively low (a few kV/cm·Torr), like in the case of a MWPC. In other geometries, for example in a parallel plate multiplier, a high constant field across the full gap would enhance photoemission and make it possible to extend the choice of gas. This is true for some other, multistage geometries, where multiplication starts at the photocathode surface. A recent example is the low-pressure UV microstrip detector [70].

6. Aging of CsI photocathodes

There are several known phenomena causing a decay in the photoemission properties of CsI: humidity, photon impact and ion bombardment. We will not discuss here other sources of decay, related for example, to surface contamination by possible impurities, or to radiation damage with neutral [10] or charged particles.

6.1 Exposure to humidity

The role of humidity on the decay in photoemission of CsI has been known for some time [15,14,13]. The decay is caused by hydrolysis of the material surface. It has been observed that the degradation of the photoemission is larger at longer wavelengths, probably due to an increase of the electron affinity [13].

Simons et al. [14] found a two-fold larger decay in QE between CsI photocathodes exposed for one hour in air of 5% and 50% humidity. Compared to a fresh photocathode, a decrease of 25% in QE at 170 nm, was observed in 100 min, at relative humidity of 25% [13]. Data of Dangendorf et al. [20] and Krizan et al. [31] speak of a decay of 50% after exposure to air for 100 min at a relative humidity of 50%.

As already discussed above (2.2), it was found that post-evaporation heat treated CsI

photocathodes have a considerably slower decay when exposed to humid air [30]. Fig. 22 shows the decay in a 50% relative humidity. Almost no decay is observed for periods below 1h; the decay is of about a factor of two after 48 h. The enhanced stability in air of heat-treated CsI films is not yet understood and is a subject of microanalysis studies. The recovery of air-exposed photocathodes by heat treatment under vacuum is discussed in 2.2. The authors of ref. [71] report on vacuum recovery at room temperature.

6.2 Aging under intense photon flux

The photocathode aging under intense photon flux is due to a photolysis process, leading to its metallization (cesiation) [72,73,74,75,24]. It is believed that following the dissociation of CsI molecules:

$$h\nu + CsI \rightarrow Cs^{+} + I + e^{-}$$

iodine atoms evaporate and the excess of cesium, with a higher electron affinity, causes a reduction in QE. Two effects support the cesiation hypothesis: a blackening of a photon-aged photocathode when exposed to air [24], due to Cs oxidation, and an enhanced sensitivity to visible light [75], due to a lower photoionization threshold of Cs (3.9 eV).

Another interpretation to the photon-induced aging, via the formation of radicals following the dissociation of H_2O contaminants and their reaction with CsI, is provided by [34].

All authors investigating the photon aging of CsI report on a two-component nature of its decay. A fast component related to surface effects and a slower one, interpreted as an aging of the bulk. Some authors found some recovery of the QE of photon-aged photocathodes when heating them to 65°-92°C [23,41]. The temperature rise was also found to slow down the photon-induced aging in vacuum [23]. A possible interpretation could be the re-establishment of the original stoichiometry of CsI due to the evaporation of Cs. The temperature effect was found to be more pronounced in a low pressure gas, leading even to an enhanced photoemission rather than to a decay [23]. In the same work, Anderson et al. have demonstrated that the photon-induced aging is slower in a gas compared to that in vacuum. They also found a reduction of aging at increased gas pressure and a dependence on the type of gas employed. Best results, at 20 Torr, are for CH_4 and i-C_4H_{10} [23] (see Fig. 23). The reduced photocathode decay in presence of a gas

could be related to a slower evaporation of the iodine atoms. Lu et al. [41] found a dependance of the photon-induced QE decay on the wavelength (see Fig. 24). As expected from the hypothesis of an increase in electron affinity, the QE decay is larger at higher wavelengths. Recent results of the Va'vra et al., of the photon aging at 1 atm of CH_4, are shown in Fig. 25.

Though several measurements of the photon-induced aging exist in the literature, many discrepancies persist in the results. The same applies to the results of ion-induced aging, as will be discussed below. The results of both aging processes are summarized in Table II, where the photon aging relates to gain =1.

For example, a 20% reduction in the QE is found in vacuum for an integrated charge of 0.5 $\mu C/mm^2$ in [23] and only 0.1 $\mu C/mm^2$ in [41]. At 20 Torr of CH_4 the same loss appears at 2 $\mu C/mm^2$ in [24] and after 25 $\mu C/mm^2$ at 20 Torr of i-C_4H_{10} in [23]. At 1 atm of CH_4 recent measurements indicate a 20% reduction in QE after 20 $\mu C/mm^2$ in [76].

For more information on the measuring procedures and conditions the reader is referred to the above mentioned references.

6.3 Aging under ion bombardment

When operated in the presence of gas multiplication, the CsI photocathode is subjected to positive ion (A^+) bombardment. Damage is caused to the photocathode surface by ion sputtering and by ion-induced dissociation of CsI:

$$A^+ + CsI \rightarrow A + CsI^+ \hookrightarrow Cs^+ + I$$

The evaporation of iodine causes an enhancement of the electron affinity of the surface due to cesiation, similar to the photon-induced effect discussed above, reflected as a loss in QE.

The ion-induced aging depends on the detector geometry, gas, pressure and gain. All four parameters define the velocity of the impinging ions and the gain defines, in addition to the electric field strength, the ion yield per converted photon. The ion aging is always combined with the photon effect and can be estimated, for a given condition, by a series of measurements at various detector gains and photon flux.

An example of the effects of photon flux and pressure is shown in Fig. 26a [24]. Here,

at very high photon flux, for equal photon flux and gain, the QE decay is larger at higher pressure; for equal pressure and gain × flux, a faster decay occurs at larger photon flux. Other measurements, at low photon flux and an equal pressure show a larger decay at high gas gain (see Fig. 26b). The latter demonstrates the importance of the photon-induced aging and its superiority, in some cases, to the ion aging. This was recently discussed in detail by the authors of ref. [41], who also found a wavelength dependence of the aging process, similar to that of the photon aging discussed above (see Fig. 27). A wavelength dependence was also measured by Krizan et al. in a recent work [31]. Their ion aging results are shown in Fig. 28.

Fig. 29 shows the results of an ion-induced QE decay of CsI at 1 atm of CH_4, of a heat-enhanced photocathode. The ion aging could be accurately measured at a gain of 10^5 at low photon flux, as to discard photon aging effects [76]. As already mentioned, there are serious discrepancies in the aging results, as reflected from table II. If we compare for example ion aging data measured at a gain of 10^5 we find in 1 atm CH_4 a 20% drop after an integrated charge of 80 $\mu C/mm^2$ in [31], and already at about 1 $\mu C/mm^2$ in [76]. It is a striking fact that the authors of [31] find an 80 times longer life time of the photocathode, though operating under about 20 times larger photon flux. Lu et al. [41] find a 20% drop in QE of a CsI photocathode on Al substrate, operated in 20 Torr of C_2H_6, also at gain of 10^5, after an integrated charge of 20 $\mu C/mm^2$.

In our opinion, as the aging effects relate to surface modifications, the discrepancies could have several origins, among them: the mode of preparation of the CsI film, the substrate, the crystalline structure, post-evaporation treatment, surface resistivity etc. A good understanding of the aging process of CsI is of prime importance for its long-term use in radiation detectors. Therefore considerable efforts should be directed to systematic studies in this field.

6.4 Long term stability under gas flow

In addition to a minimal decay under photon flux and gas multiplication it is important to have a good knowledge of the long term stability of CsI films in gas media. Most works in this field report on a rather stable, short or medium term, behaviour under storage in dry gas or in a moderate vacuum (desiccators). Piuz et al., have gained so far considerable

experience in long term operation of CsI-based wire chambers in RICH. They report on the conservation of the QE of a CsI pad electrode mounted in a wire chamber made of epoxy resin frames and kept under CH_4 flow for 6 months.

Recent systematic measurements made at Saclay, show an impressive stability of a CsI photocathode made on a Cu/Ni substrate, kept in a MWPC for more than 8 months. The photocathode was not subjected to a heat enhancement treatment. The detector was constantly kept under voltage, at 1 atm of a flow of CH_4 and gain of 10^5. It was occasionally illuminated and characterized. As shown in fig. 30, the stability of response appears even at 215 nm [77]. It is a very encouraging fact because a photocathode deterioration usually starts at longer wavelengths.

7. Other topics of interest

In addition to the considerable amount of CsI data presented above, other topics of interest have been investigated and will be briefly discussed in the following.

An interesting observation was made by Seguionot et al. [22] of an enhanced photoemission of TMAE-adsorbed CsI films. The QE value of these films was found to be superior to that of CsI and that of TMAE. The phenomenon of TMAE-enhanced QE of CsI was confirmed by other groups [51,23,39]. However, it should be noted that the TMAE adsorption effect is unstable, which makes it impractical for current use in detectors. Unless fresh TMAE is constantly added to the gas mixture, the adsorbed film is removed either by flowing gas or by pumping [39].

Porous CsI UV-photocathodes have been so far only slightly investigated. Some minor enhancement in the emission properties was found in [36] while the authors of [10] did not find any noticeable affect in porous films prepared at the same origin. The lack of an expected enhancement, due to high electric fields in the CsI pores, could be explained by possible damage to the porous layer, by humidity, during transfer into the chamber. Though being very fragile, porous CsI films could be of interest and should be farther investigated.

Photoemission into liquid and solid noble gases has been investigated by Aprile et al. These authors discovered that at 220 nm, close to the photothreshold of CsI, the photoemission into liquid Xe and into liquid Kr is 3 and 2 times larger, respectively,

compared to that into vacuum, as shown in fig. 31 [60]. The phenomenon is explained by a reduction of the electron affinity in the liquid-solid interface. It is interesting to note that this phenomenon compensates for the electron backscattering into the liquid. Measurements of photoemission into solid Xe have shown a further increase in quantum efficiency compared to that in liquid Xe [79].

Parameters like transmission [28,34] and reflection [45] coefficients of CsI films were measured by some groups as a function of thickness and photon wavelength; angular incidence effects on the QE were investigated in [80].

The properties of semitransparent CsI photocathodes were investigated in detail by the authors of ref. [28]. In this mode, due to the relatively short electron escape length [4] (see Fig. 2), the thickness of the photocathode is a crucial parameter, as shown in fig. 32. At the optimal thickness, of 13 nm, the quantum efficiency at 170 nm reaches values of the order of 18% [28]. This is to be compared with about 3% in ref. [3] and 7% in ref. [81].

As mentioned in the introduction, it would probably be preferable from the points of view of QE and simplicity to employ thicker CsI films deposited on mesh electrodes for devices operating in a transmission geometry [3,16]. In such geometries, CsI on thin wire electrodes could benefit from an additional field-enhanced emission [53]. Aging studies of CsI under intense gamma irradiation [10] show no damage below 550 Gy, both for films made of crystal and powder raw materials. A reduction in photoemission by the order of a factor of two, in the spectral range of 140-210 nm, was observed after irradiation at 4500 Gy [10].

In parallel to the experimental research, modelling of electron transport and emission from CsI films has been undertaken [4,28]. For example, recent calculations remarkably reproduce QE data of semitransparent and reflective photocathodes as shown in fig. 33 [4]. The model developed in ref. [4] provides electron emission spectra and the electron escape length, also in other alkali halides. Fig. 2 shows the superior escape length of CsI compared to that of other alkali halide materials, which explains its higher QE values.

Other models, of the field enhanced emission from CsI, are in good agreement with experimental results and support the hypothesis of a reduction in electron affinity, similar to the Schottky effect in metals [53]. The modelling of photoelectron backscattering from different gases [69] confirms the experimental results measured at

the laboratory and in a CsI-based RICH device.

8. Summary

We have reviewed the properties of CsI photoemissive films, which have lately attracted considerable interest. The article provides a historical review of the field, tries to explain various phenomena and anomalies observed, and puts an emphasis on some persisting mysteries and open questions.

We can see with satisfaction that the yield of mysteries constantly decreases due to the impressive and tedious research efforts invested by numerous groups. This permits a more profound understanding of the physical processes involved in surface photoemission from CsI.

The production technique of large area CsI films seems to be mastered. To our satisfaction, recent QE data from large area CsI-based UV-RICH devices approach that of laboratory samples [26 and references therein, 82]. This was made possible due to numerous studies combining electrical an microanalysis techniques.

Methods are being looked for to enhance the QE of CsI and to understand its aging process under photon and ion bombardment. It should be remembered that from these two points of view, TMAE vapours, though less practical and often not suitable for photon detection under very large flux, have still some superiority.

Charging up effects at high radiation flux have to be seriously investigated and understood. The role of the substrate and the mechanism of heat-enhancement of the QE should be clarified. Recent studies of the heat-enhancement of the QE of some photosensitive materials could provide some new hints in this matter [83]. In addition to the intensive research in photoemission from CsI, considerable efforts are directed towards the search of other photosensitive materials [5 and references therein, 71,84,85,86] including visible photocathodes capable of operating under gas multiplication. Among other, CsI was used to protect air-sensitive films [85]. Recent works have as an approach the coating of air-sensitive photo emitter with inert insulating films [42,87].

I would like to thank Dr. R. Chechik for her close collaboration in this field and her appreciable help in preparing this manuscript. Fruitful discussions with Dr. A. Buzulutskov, Dr. F. Piuz and Dr. J. Va'vra are deeply acknowledged. Special thanks to many of my colleagues and friends, whose important contributions in the field of photoemission from CsI made this work possible. The help of Mrs. H. Fischer in preparing this manuscript with patience and devotion is well appreciated and acknowledged.

Many of the results of the Weizmann Institute group, presented here, originate from a research work supported by the Foundation Mordoh Mijan de Salonique, The Israel Academy of Sciences and Humanities, The US-Israel Binational Science Foundation, The Commission of the European Communities and The Israel Ministry of Science and Arts.

The author is the W.P. Reuther Professor of research in the peaceful uses of atomic energy.

References

1. E.A. Taft and H.R. Philipp, Phys. Chem Solids **3** (1957) 1.
2. G.R. Carruthers, Appl. Opt. **8** (1969) 633.
3. G.F. Carruthers, Appl. Opt. **14** (1975) 1667.
4. A. Akkerman, T. Boutboul, A. Breskin, R. Chechik and A. Gibrekhterman, J. Appl. Phys. **76** (1994) 4656.
5. P. Miné, Nucl. Instrum. and Meth. **A343** (1994) 99 and references therein.
6. R.A. Holroyd, J.M. Preses, C.L. Woody and R.A. Johnson, Nucl. Instrum. and Meth. **A261** (1987) 440.
7. A. Breskin, Secondary emission gaseous detectors; a new class of radiation imaging devices. Preprint WIS-95/3/Jan.-PH. Nucl. Phys. B (Proc. Supp.) in press.
8. A.H. Sommer, Photoemissive materials, Willey NY, 1968.
9. J. Va'vra, A. Breskin, A. Buzulutskov, R. Chechik and E. Shefer, Resistivity of CsI photocathodes, in preparation.
10. G. Malamud, P. Miné, D. Vartsky, A. Breskin and R. Chechik, Nucl. Instrum. and Meth. **A335** (1993) 136.
11. M.R. Sims, A. Peacock and B.G. Taylor, Nucl. Instrum. and Meth. **221** (1984) 168.
12. C. Martin and S. Bowyer, Appl. Opt. **21** (1982) 4206.
13. D.G. Simons, G.W Fraser, P.A.J. De Korte, J.F. Pearson and L. De Jong, Nucl. Instrum. and Meth. **A261** (1987) 579.
14. D.G. Simons, P.A.J. De Korte, A. Peacock, A. Smith and J.A.H. Bleeker, IEEE Trans. Nucl. Sci. **NS-32** (1985) 345.
15. L. Heroux, W.J. McMahon and H.E. Hinteregger, Appl. Opt. **5** (1966) 1338.
16. T. Ypsilantis, presented at the 1979 IEEE Nucl. Sci. Symposium. Unpublished work.
17. D.F. Anderson, IEEE Trans. Nucl. Sci. **NS-28** (1981) 842
18. G. Comby, P. Mangeot, P. Prugne, J.F. Chalot, E. Coulareau, J. Quidort, J.J. Beauval and J. Tichit. Nucl. Instrum. and Meth. **176** (1980) 313.
19. J.F. Chalot, G. Comby and J. Quidort, IEEE Trans. Nucl. Sci. **NS-29** (1982) 211.
20. V. Dangendorf, A. Breskin, R. Chechik, and H. Schmidt-Böcking, Nucl. Instrum. and Meth. **A289** (1990) 322.
21. G. Charpak, V. Peskov, D. Scigocki and V. Valbis, Proc. Int. Symp. on Particle

Identification at High Luminosity Hadron Colliders (ed. T.G. Gouraly and I.G. Morfin) FNAL, IL, USA (1989) p. 295 and G. Charpak, V. Peskov and D. Scigocki, Proc. of the 8th Workshop on New Detectors in Future Supercolliders, ERICE, Oct. 1989. Preprint CERN-EP/90-41.

22. J. Seguinot, G. Charpak, Y. Giomataris, V. Peskov, J. Tischauser and T. Ypsilantis, Nucl. Instrum. and Meth. **A297** (1990) 133 and T. Ypsilantis, Proc. of the ECFA Workshop on Instrum. Tech for High Luminosity Hadron Colliders, Barcelona, Sept. 1989. Preprint CERN 89-10.
23. D.F. Anderson, S. Kwan, V. Peskov and B. Hoeneisen, Nucl. Instrum. and Meth. **A323** (1992) 626.
24. V. Dangendorf, A. Breskin, R. Chechik and H. Schmidt-Böcking, Nucl. Instrum. and Meth. **A308** (1991) 519.
25. G. Charpak, P. Fonte, V. Peskov, F. Sauli, D. Seigocki and D. Stuart, Nucl. Instrum. and Meth. **A307** (1991) 63.
26. F. Piuz, RICH with CsI photocathodes, Invited talk at the second workshop on RICH, Uppsala, June 1995. These proceedings, and references therein.
27. The Proc. of the First Workshop on RICH, Bari, Italy, Nucl. Instrum and Meth. **A343** (1994) and references therein.
28. C. Lu and K. McDonald, Nucl. Instrum. and Meth. **A343** (1994) 135.
29. J. Berger et al. Nucl. Instrum. and Meth. **A360** (1995) 411.
30. J. Almeida et al., Microanalysis surface studies and photoemission properties of CsI photocathodes. Preprint WIS-95/14/March-PH, Nucl. Instrum. and Meth., in press.
31. P. Krizan, M. Cindro, V. Cindro, S. Korpar, G. Omahen, A. Stanovnik and M. Staric, Measurements of the quantum efficiency of CsI photocathodes in a MWPC. Preprint IJS-DP-7087, Oct. 1994.
32. D.F. Anderson, S. Kwan and V. Peskov, Nucl. Instrum. and Meth. **A326** (1993) 611.
33. G. Malamud, P. Miné, D. Vartsky, B. Equer, P. Besson, Ph. Bourgeois, A. Breskin and R. Chechik, Nucl. Instrum. and Meth. **A348** (1994) 275.
34. P. Maier-Komor, B.B. Bauer, J. Friese, R. Gernhäuser, P. Kienle, H.J. Körner, G. Montermann and K. Zeitelhack, Nucl. Instrum. and Meth. **A362** (1995) 183.
35. J. Friese, Private communication.

36. R. Aleksan, P. Besson, Ph. Bourgeois, P. Garganne and J.P. Robert, Nucl. Instrum. and Meth. **A340** (1994) 293.
37. G.W. Goetze, A.H. Boerio and M. Green, J. Appl. Phys. **35** (1964) 482.
38. D.F. Anderson, B. Hoeneisen, S. Kwan and V., Perskov. FNAL TM-1753, 1991.
39. D.C. Imrie, A.H. Moghul, K. Wells, G. Charpak and V. Peskov, Nucl. Instrum. and Meth. **A310** (1991) 122.
40. H. Brauning, A. Breskin R. Chechik, P. Miné and D. Vartsky, Nucl. Instrum. and Meth. **A327** (1993) 369.
41. C. Lu, B. Cheng, K. McDonald, D.R. Marlow, E.J. Prebys and R.L. Wixted. Characterization of CsI photocathodes for use in a fast RICH detector. Preprint Princeton/HEP/94-10, June 1994.
42. A. Breskin, A. Buzulutskov and R. Chechik, IEEE Trans. Nucl. Sci. **42** (1995) 298.
43. J. Almeida et al., Review of the development of CsI photocathodes for application to large RICH detectors. Preprint CERN-PPE/95-63, Nucl. Instrum. and Meth. in Phys. Res. A in press.
44. J. Almeida et al., Nucl. Instrum. and Meth. **A361** (1995) 524 and references therein.
45. A. Braem et al., Nucl. Instrum. and Meth. **A343** (1994) 163.
46. G.D. Hallewell, Nucl. Instrum. and Meth. **A343** (1994) 250.
47. P. Miné, private communication.
48. P. Dorenbos, J.T.M. de Haas, R. Visser, C.W.E. Van Eijk, and R.W. Hollander, Nucl. Instrum. and Meth. **A325** (1993) 367.
49. A. Breskin, R. Chechik, D. Vartsky, G. Malamud and P. Miné, Nucl. Instrum. and Meth. **A343** (1994) 159.
50. P. Besson, Ph. Bourgeois, P. Garganne, J.P. Robert, L. Giry and Y. Vitel, Nucl. Instrum and Meth. **A344** (1994) 435.
51. S. Kwan and D.F. Anderson, Nucl. Instrum. and Meth. **A309** (1991) 190.
52. A. Breskin, A. Buzulutskov, R. Chechik, D. Vartsky, G. Malamud and P. Miné, Nucl. Instru. and Meth. **A344** (1994) 537.
53. A. Buzulutskov, A. Breskin and R. Chechik, J. Appl. Phys. **77** (1995) 2138.
54. R. Arnold, E. Christophel and J.L. Guyonnet, Preprint CRN/HE 91-06, CRN Strasbourg.

55. N.S. Lockyer, J.E. Millan, C. Lu, K.T. McDonald and A. Lopez, Nucl. Instrum. and Meth. **A332** (1993) 142.

56. F. Piuz, A. Braem, G. Paic, R.S. Ribeiro and T.D. Williasm, Nucl. Instrum. and Meth. **A333** (1993) 404.

57. B. Surrow, et al., Nucl. Instrum. and Meth. **A355** (1995) 342.

58. R. Aleksan et al., Nucl. Instrum. and Meth. **A343** (1994) 173.

59. M. Staric, A. Stanovnik and P. Krizan, Nucl. Instrum. and Meth. **A307** (1991) 145.

60. E. Aprile, A. Bolotnikov, D. Chen, R. Mukherjee, F. Xu, D.F. Anderson and V. Peskov, Nucl. Instrum. and Meth. **A343** (1994) 129.

61. L.B. Loeb, Basic processes in gaseous electronics, Univ. of California Press, Berkeley, 1961.

62. V. Peskov, Sov. Phys. Tech. Phys. **32** (1977) 335.

63. D.F. Anderson, R. Bouclier, G. Charpak, S. Majewski and G. Kneller, Nucl. Instrum. and Meth. **217** (1983) 217.

64. G. Charpak, W. Dominik, F. Sauli and S. Majewski, IEEE Trans. Nucl. Sci. **NS-30** (1983) 134.

65. V. Cindro, H. Ehrlichmann, S. Korpar, P. Krizan, A. Stanovnik and M. Staric, Nucl. Phys. B (Proc. Supp.) **32** (1993) 230.

66. C. Lu, K.T. McDonald and Y. Zhu, Nucl. Instrum. and Meth. **A334** (1993) 328.

67. E.M. Gushchin, A.N. Lebedev, S. V. Somov, V.P. Protasov, M.K. Timofeev and G.I. Tipografshchik, Instr. Exp. Tech. **36** (1993) 754.

68. A. Breskin, A. Buzulutskov, R. Chechik, A. Di Mauro, E. Nappi, G. Paic and F. Piuz, Field-dependent photoelectron extraction from CsI in different gases. Preprint WIS-95/4/Feb.-PH. Nucl. Instrum. and Meth A, in press.

69. A. Di Mauro, E. Nappi, F. Posa, A. Breskin, A. Buzulutskov, R. Chechik, S.F. Biagi, G. Paic and F. Piuz, Photoelectron backscattering effects in photoemission from CsI into gas media. Preprint WIS-95/34/Aug.-PH. These proceedings.

70. A. Breskin, E. Shefer, R. Chechik and A. Pansky, Nucl. Instrum. and Meth. **A345** (1994) 205.

71. R. Enomoto, T. Sumiyoshi and Y. Fujita, Nucl. Instrum. and Meth. **A343** (1994) 117.

72. R.L. Verma, J. Phys. **D11** (1978) 63.

73. I.P. Antoniv, N.N. Vaschenyuk, Y.A. Levitskaya, V.A. Matykhin and N. Tsal, Radio Eng. Electron Phys. **21** (1976) 82.
74. V. Dangendorf, A. Breskin, R. Chechik and H. Schmidt-Böcking, in Instrum. in Astronomy VII (ed. D.L. Crawford), Proc. SPIE **1235** (1990) 896.
75. B. Hoeneisen, D.F. Anderson and S. Kwan, Nucl. Instrum. and Meth. **A302** (1991) 447.
76. J. Vav'ra, A. Breskin, A. Buzulutskov, R. Chechik and E. Shefer, Aging of CsI-based photocathodes in gaseous MWPC detectors. In preparation.
77. R. Aleksan et al., Saclay, Detection of Cherenkov UV-light with CsI photocathodes in a MWPC. In preparation.
78. A. Buzulutskov, A. Breskin, R. Chechik and D. Vartsky, Nucl. Instrum. and Meth. **A350** (1994) 406.
79. E. Aprile, A. Bolotnikov, D. Chen, F. Xu and V. Peskov, Nucl. Instrum. and Meth. **A353** (1994) 55.
80. P. Miné, G. Vasileiadis, G. Malamud, D. Vartsky, A. Breskin and R. Chechik, Nucl. Instrum. and Meth. **A360** (1995) 430.
81. G. Charpak, I. Gaudean, V. Peskov, D. Scigocki, F. Sauli and D. Stuart, Nucl. Instrum. and Meth. **A333** (1993) 391.
82. J.L. Guyonnet et al., Fast RICH technique for proximity focussing LiF or CaF_2 radiators. These proceedings.
83. A. Buzulutskov, A. Breskin and R. Chechik, Heat enhancement of the photoyield from CsI, NaI and CuI photocathodes. Preprint WIS-95/37/Aug.-PH. Nucl. Instrum. and Meth, in press.
84. D.F. Anderson, S. Kwan and V. Peskov, Nucl. Instrum. and Meth. **A343** (1994) 109.
85. V. Peskov, A. Borovik-Romanov, T. Sokolova and E. Silin, Nucl. Instrum. and Meth. **A353** (1994) 184.
86. V. Peskov and E. Silin, High efficiency photocathodes for gaseous detectors of visible photons. Preprint CERN/AT/95-07(ET), April 1995. Nucl. Instrum. and Meth., in press.
87. A. Buzulutskov, A. Breskin, R. Chechik and J. Va'vra, Study of photocathode protection with thin dielectric films. Preprint WIS-95/32/July-PH. These proceedings.

Figure Captions

Fig. 1 Typical quantum yields versus wavelength for reflective alkali halide photocathodes. Shown for comparison is a typical quantum yield curve for a semitransparent CsI photocathode deposited on a LiF window (CsI S.T.) [2].

Fig. 2 Calculated escape probability for electrons with initial energy of 1 eV, as function of their creation depth in CsI, NaCl and KCl. The calculations are based on a microscopic model of electron transport in alkali halides [4].

Fig. 3 Comparison of the quantum yields of typical reflective and semitransparent (S.T.) photocathodes of CsI and KBr, from NRL (Naval Research Laboratories) measurements [3].

Fig. 4 a) QE as a function of wavelength, measured in 20 Torr Methane, for CsI photocathodes produced from scintillator (Sc) and powder (P), both vacuum deposited (V) and spray deposited (Sp) [32].
b) QE in vacuum as the function of wavelength of CsI photocathodes prepared with two different monocrystals: C1, C2 and two different powders: P1, P2. The vacuum was $2x10^{-5}$ mbar and the electric field 750 V/cm [33].

Fig. 5 The measured quantum yields versus the photon wavelength of a 500 nm thick CsI photocathode after 1, 17, and 41 h of methane gas-flow through the chamber. The solid line without data points is the TMAE gas-phase yield, and the dash-dotted line is the Carruthers vacuum photocathode yield [22].

Fig. 6 QE as a function of time of a freshly deposited, 0.5 nm thick CsI photocathode, with a 40 l/min flow of methane. At 20 hours the photocathode is heated to 97° C , resulting in the enhancement of the photoyield [38].

Fig. 7 a) QE spectra of a 500 nm thick CsI film on stainless steel substrate, after heating to 60°C at 10^{-7} Torr, as function of the heating time [42].
b) QE spectra of CsI, in vacuum of 10^{-7} Torr, immediately after evaporation, after 24h at room temperature and after 20h at 60° C.

Fig. 8 Atomic Force Microscope image taken at atomic scale, of CsI on a printed board circuit/Ni/Au substrate. On the right is the inverse Fourier transform, showing the lattice periodicity [30].

Fig. 9 Atomic Force Microscope images of CsI evaporated on Si substrates. The grain size varies with the thickness of the C intermediate layer, due to variation of wetting and smoothness. a) no C, b) 100 Å of C, c) 800 Å of C. The images on the left side provide the third coordinate depth scale [30].

Fig. 10 Scanning Electron Microscope images of CsI evaporated on standard printed board circuit with chemically deposited Au (left) and Ni/Au (right). Our study

shows that the top sample has very low QE and CsI chemically reacts with Cu and dissociates. The bottom sample shows high QE and stable CsI crystalline structure [44].

Fig. 11 VUV-PEEM (photoemission electron emission microscope) micro images of photoemission from CsI deposited on different substrates. The differences in uniformity and emission intensity are evident [44].

Fig. 12 The differences in the extinction coefficient of TMAE vapors, reflecting the photoabsorption, measured by various groups [28].

Fig. 13 The ratio between the quantum efficiency measured by Breskin et al, using a NIST calibrated vacuum photodiode, and that supplied by Hamamatsu, for four different photomultipliers of the R1460 series. Serial numbers are indicated in the figure [49]. Note that the producer's underestimation of the QE reaches factors up to 2.5.

Fig. 14 QE spectra of CsI photocathodes deposited on printed board pad electrodes of a UV detector, extracted from beam-test data of a RICH detector, compared to the RD-26 reference QE measured on stainless steal substrate in vacuum in the laboratory (see Fig. 15). Details are given in Ref. 26, 43.

Fig. 15 The QE of heat-enhanced CsI photocathodes (best and mean of 5), measured at the Weizmann Institute and at Ecole Polytechnique. The quantum efficiency of TMAE [6], and of CsI (Seguinot et al. [22] at 1 atm CH_4 and Anderson et al. [23] at 20 Torr CH_4) are shown for comparison [49].

Fig. 16 Measured quantum efficiency of a CsI photocathode using a NIST-calibrated PMT as reference. Also shown are older results using TMAE as reference [28], and results from Breskin et al [49] using a calibrated PMT as reference [41].

Fig. 17 The measured QE spectra of one 500 nm thick and two 900 nm thick CsI photocathodes, on Sn/Pb substrates (dotted points) compared to the QE values of Seguinot et al (dashed line). The measurements were performed in a MWPC operated at room temperature with 1 atm CH_4. The QE was measured in pulse counting mode, normalized to a calibrated PMT [31].

Fig. 18 A schematic view of the experimental setup to measure field-enhancement of photoemission. The photocurrent from the CsI multiwire photocathode (10 nm in diameter wires), induced by gamma-ray scintillation in BaF_2 or $KMgF_3$ crystals or by a UV-lamp, is measured in vacuum, as function of the electric field [78].

Fig. 19 The field-enhancement of photoemission from CsI, measured in the setup shown in fig. 18. (a) Normalized photocurrent from CsI as a function of the electric field strength for BaF_2 and $KMgF_3$ scintillators; each data set is normalized to the point at the lowest field value. (b), (c) Normalized QE of CsI as a function of the

electric field strength at 160 nm, 185 nm and above 200 nm. Errors are smaller than the point size [78].

Fig. 20 Photoemission into gas. The relative quantum efficiency of CsI, measured with the photon counting technique at about 190 nm, and the gas gain, as a function of the reduced electric field in a) He/CH_4 (95/5) and He/i-C_4H_{10} (95/5), 800 Torr; the QE data points are normalized to the last three points averaged. (b) CH_4 /i-C_4H_{10} (95/5) at 200 and 400 Torr; the QE data points are normalized to the points at E/p≥ 30 V/cm·Torr, averaged [68].

Fig. 21 The ratio of the DC photocurrent from CsI at 185 nm, in CH_4 and in He- and Ar-based gas mixtures at atmospheric pressure, to the photocurrent in vacuum (measured at the same absolute electric field values), as a function of the reduced electric field in the gas. Note that in the charge collection mode, (E/p<4 V/cm·Torr) the photocurrent in CH_4 (and CH_4-based mixtures, not shown here) and in some Ar-based mixtures, approaches that of vacuum. He-based mixtures would considerably reduce the photocurrent from CsI. [52, 68 and 69].

Fig. 22 The decay of the QE of CsI films evaporated on Ni/Au-coated printed circuit board under exposure to air, at a relative humidity of 35% [30].

Fig. 23 CsI photocathode photon-induced aging (no multiplication). (a) Normalized current as a function of total collected charge for CsI photocathodes aged in vacuum and in four different pressures of isobutane. (b) idem, in vacuum and in five different gases at 20 Torr. (c) idem, in vacuum and 20 Torr of isobutane at 25 and 65°C. [23].

Fig. 24 Photon-induced aging of a CsI photocathode in vacuum, without charge multiplication, as function of the accumulated charge, for different wavelengths [41].

Fig. 25. Photon-induced aging of CsI, deposited on a stainless steel substrate, in 1 atm CH_4, without multiplication, as function of the accumulated charge. The photon wavelength is about 185 nm, and photon flux density is about 10^{10} photons/mm^2·s. [76].

Fig. 26 Aging under gas multiplication, effects of pressure and gain.
(a) The decay of the CsI quantum efficiency, measured with a photocathode installed in a double stage avalanche chamber, for different CH_4 pressures and UV-photon flux, as function of the accumulated charge on the second amplification stage. The irradiated area is about 50 mm^2; (a) more than $3 \cdot 10^{11}$ photons/mm^2·s, p=100 Torr, gain at the first stage 100, second stage 1. (b) more than $3 \cdot 10^{11}$ photons/mm^2·s, p=20 Torr, gain at the first stage 100, second stage 1. (c) more than $3 \cdot 10^{13}$ photons/mm^2·s, p=20 Torr, no charge gain (photon aging only).
(b) The decay of the CsI quantum efficiency, measured as above, due to photon

flux and positive ion feedback as function of the charge accumulated on the second amplification stage. Total chamber gain is 350, 10 Torr CH_4, photon flux = 10^8 photon/mm^2·s. The irradiated surface is 50 mm^2. (a) gain: first stage 1, second stage 350. (b) gain: first stage 350, second stage 1 [24].

Fig. 27 The aging of a CsI photocathode in 20 Torr C_2H_6 in a MWPC, under gas gain of 10^5, as function of the total accumulated charge, for different wave lengths [41].

Fig. 28 The relative decay of the photocurrent from a CsI photocathode in a MWPC, at 1 atm CH_4, gain= 10^5, as function of the accumulated charge. The photocathode is 900 nm thick CsI on Sn/Pb coated printed circuit board substrate. I_0=0.017 mC/h [31].

Fig. 29 Ion-induced aging of a CsI photocathode mounted in a MWPC, operated with 1 atm CH_4, gain=10^5, as function of the accumulated charge. Photons are at 185 nm, photon flux is $6 \cdot 10^3$ photons/mm^2·s [76].

Fig. 30 Long term stability of a CsI photocathode. The quantum efficiency measured in 1 atm Methane as a function of time (Cu/Ni substrate) [77].

Fig. 31 Photocurrent induced by UV light (220 nm) as a function of electric field from a reflective, 5000 Å thick, CsI photocathode in vacuum as well as in liquid Xe, and liquid Kr [79].

Fig. 32 The QE of a semitransparent CsI photocathode, as function of its thickness, for five wavelengths [28].

Fig. 33 (a) The QE of a semitransparent CsI photocathode versus its thickness at photon wavelengths of 170 and 180 nm. The full curves are model calculations, the dashed curves are data from ref. 28.
(b) The QE of a 500 nm thick reflective CsI photocathode, versus wavelength. The hollow symbols are model simulations and the curve is experimental data from ref. 49 [4].

Table captions

I. A summary of selected data on the quantum efficiency of CsI. Provided are the methods of measurement, the reference for the light flux estimation, the substrate material, information about heat-enhancement and the average QE value at 170 nm. In cases where data were measured at other wavelengths, an extrapolation was made to 170 nn (data in brackets).

II. A summary of aging studies of CsI photocathodes in vacuum and gas media under charge collection (G=1) or multiplication. The photocathode lifetime is defined in terms of the collected charge per unit area, inducing a 20% loss in QE.

Table I

GROUP	METHOD/ MEDIUM	REF. FOR QE	SUBSTRATE	post evaporation HEAT ENHANCEMENT	QE (170 NM)
CARRUTHERS [3] SRL, Washington	Vacuum UV-camera	unknown	unknown	No	30%
SIMONS, FRASER et al. [13] Leicester	Vacuum MCP	Calibrated (NBS) PM, Channeltron	MCP glass	No	10%
SEGUINOT et al. [22] CERN	Photocurrent CH_4, 1 atm	TMAE gas	Stainless steel	System kept always at 40°C	best 35% average 28%
ANDERSON, PESKOV et al. [32] FNAL	photocurrent vac./gas, + low pressure PPC	TMAE gas	Al	yes, 65°C	best 34% (CsI Scintillator)
BRESKIN et al. [49] Weizmann Institute	photocurrent Vac. or CH_4	calibrated PM, with NIST vac. photodiode	Stainless steel and Cu/Ni, Cu/Ni/Au	yes, 60°C in high vacuum (4h)	>100 samples 30%
MINÉ et al. [49] Ecole Polytechnique	photocurrent Vac. or CH_4	calibrated PM, with NIST Vac. photodiode	stainless steel	yes, 60°C in high vacuum	tens samples 30%
LU et al. [41] Princeton	photocurrent	NIST Vacuum photodiode	Al	No	20% at 180 nm ($\Rightarrow\sim$ 27%)
KRIŽAN et al. [31] Ljubljana	MWPC 1 atm CH_4 also RICH	non-calibrated PM and Npe in RICH	Cu, Cu/Sn/Pb	yes, 65°C in CH_4	70 samples 35% (Sn/Pb) 22% (Cu)
BESSON et al. [77] Saclay	MWPC, 1 atm and RICH	calibrated PM and RICH	Cu/Ni	No	18% at 180 nm ($\Rightarrow\sim$ 23%)
PIUZ et al. [26,43] CERN (RD26)	RICH	Npe in RICH	Cu/Ni Cu/Ni/Au	yes, 60°C 12h in high vac.	23-28% t
HEMMICK et al. [57] Stony Brook	low pressure PPC and RICH	non-calibrated PM	Cu/Ti/Al	yes, 52°C 12 h in high vac.	$\sim$ 23% at 188 nm ($\Rightarrow\sim$ 30%)

Table II

GROUP	FLUX [photons/mm^2·s]	FLUX current: [pA/mm^2]	DETECTOR	GAS/PRESSURE	GAIN	COLLECTED CHARGE 20% LOSS IN QE [μC/mm^2]
DANGENDORF et al.	10^8	700	PPC	CH_4, 10 Torr	350	0.4
(Weizmann)	10^{11}	$2{\cdot}10^5$		20 Torr	100	4
[24]	10^{11}	$2{\cdot}10^5$		100 Torr	100	8
	10^{13}	$2{\cdot}10^5$		20 Torr	1	2
ANDERSON et al.		70	PPC	Vacuum	1	0.5
(FNAL)		600		i-C_4H_{10}, 20 Torr	1	25
[23]						
LU et al.		14,000	MWPC	C_2H_6, 20 Torr	300	15
(Princeton)		150			10^4	25
[41]		300			10^5	20
		57		Vacuum	1	0.1
KRIŽAN et al.	10^5	300	MWPC	CH_4, 1 atm.	10^5	80
(Ljubljana)						
[31]						
VA'VRA et al.	$6{\cdot}10^3$(185 nm)	16	MWPC	CH_4, 1 atm.	10^5	<1
(Weizmann)	10^{10}	300			1	20
[76]						

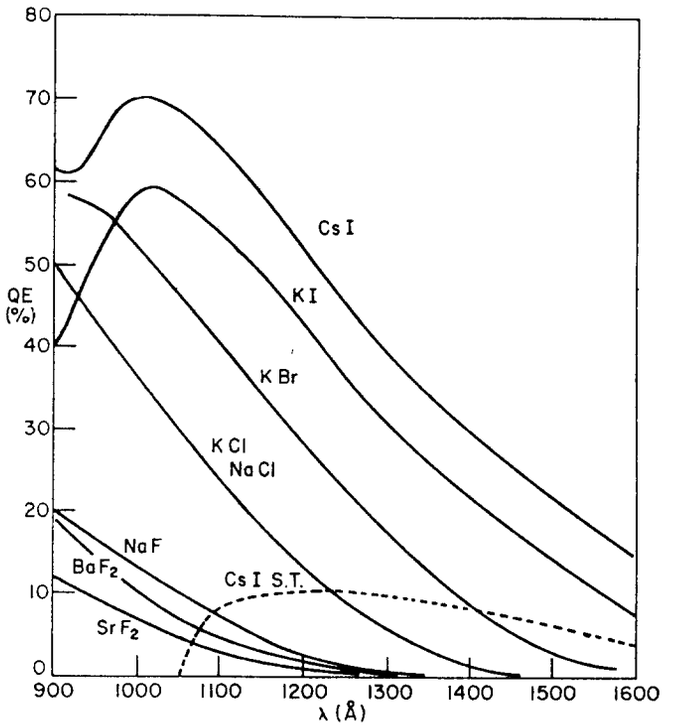
80
70
60
50
40
30
20
10
0
QE
(%)
Cs I
K I
K Br
K Cl
Na Cl
Na F
Ba F2
Cs I S.T.
Sr F2
900
1000
1100
1200
1300
1400
1500
1600
λ (Å)

Fig. 1

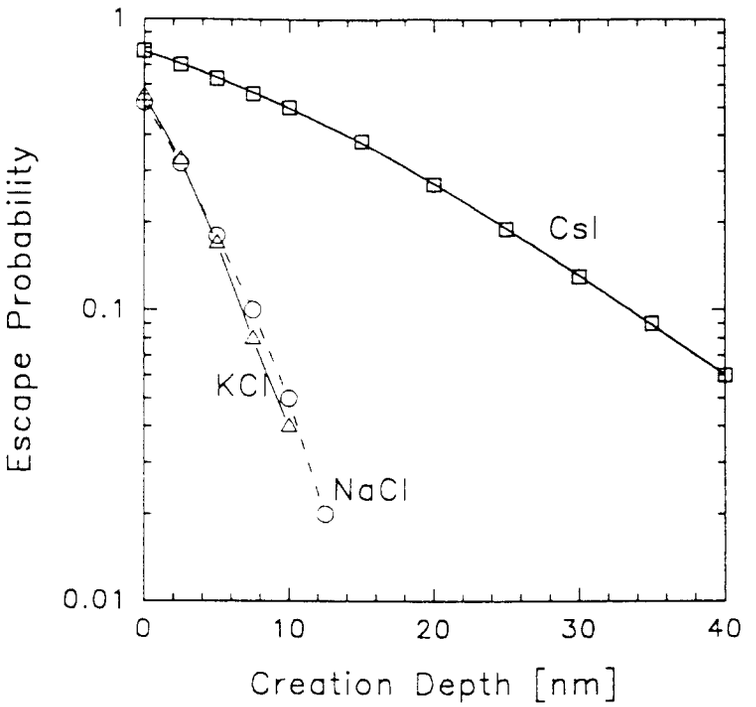
1
0.1
0.01
Escape Probability
CsI
KCl
NaCl
0
10
20
30
40
Creation Depth [nm]

Fig. 2

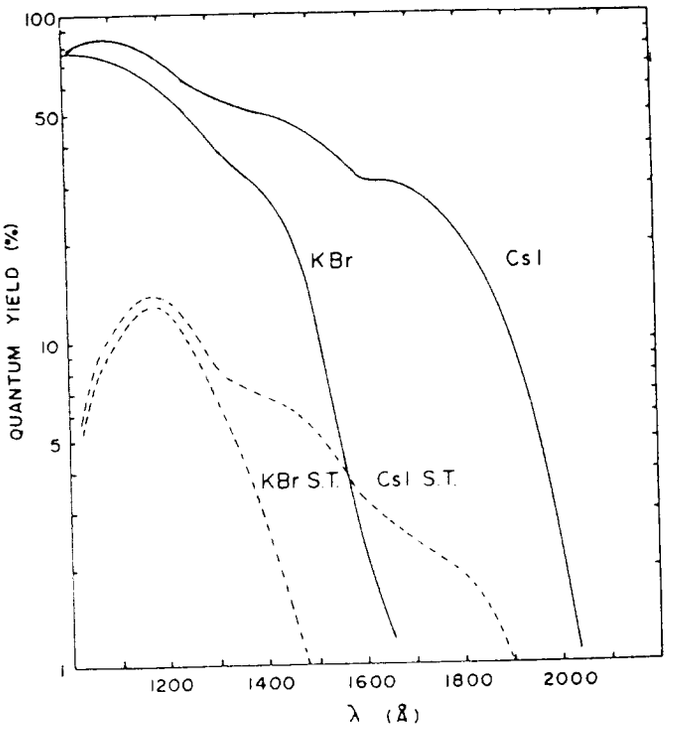
100
50
10
5
1
QUANTUM YIELD (%)
KBr
CsI
KBr S.T.
CsI S.T.
1200
1400
1600
1800
2000
λ (Å)

Fig. 3

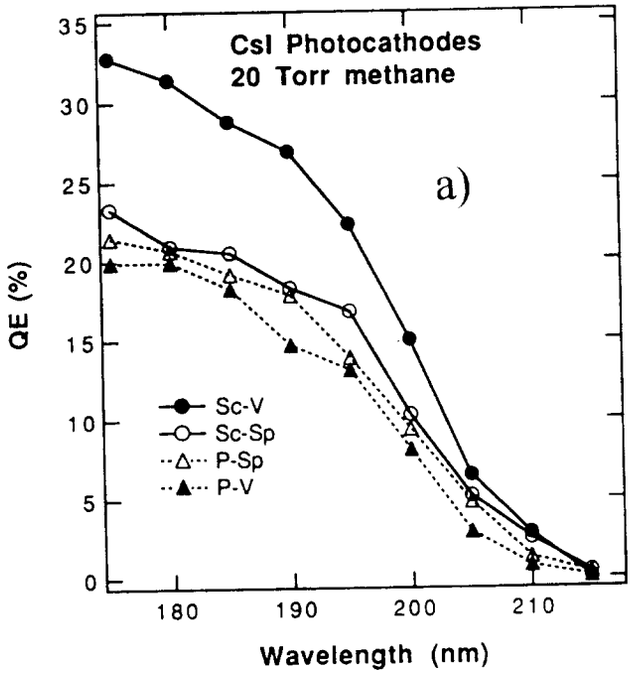
CsI Photocathodes
20 Torr methane
a)
QE (%)
Sc-V
Sc-Sp
P-Sp
P-V
Wavelength (nm)

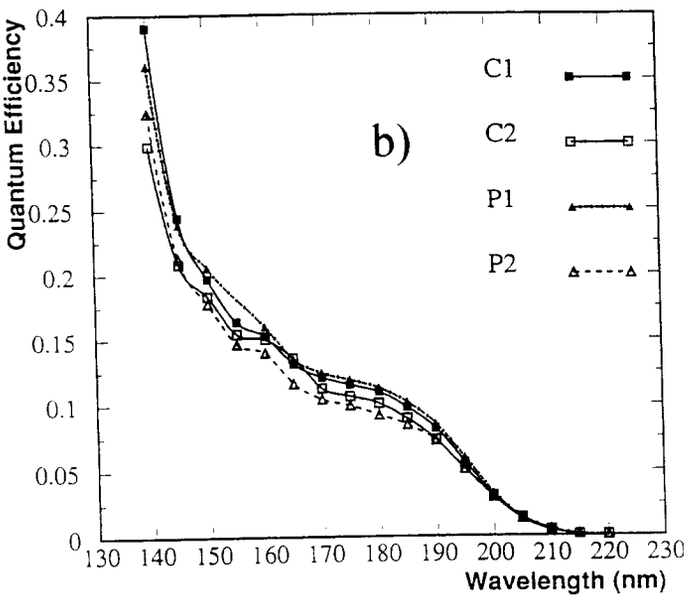
Quantum Efficiency
b)
C1
C2
P1
P2
Wavelength (nm)

Fig. 4

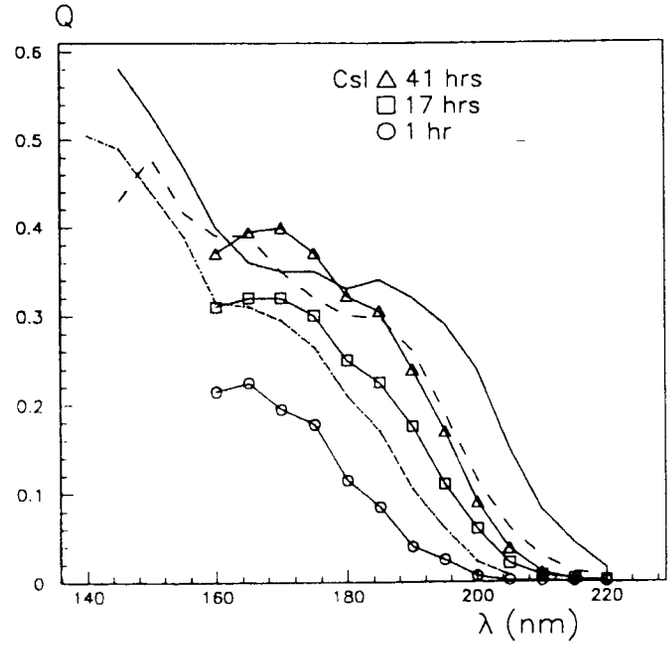

Fig. 5

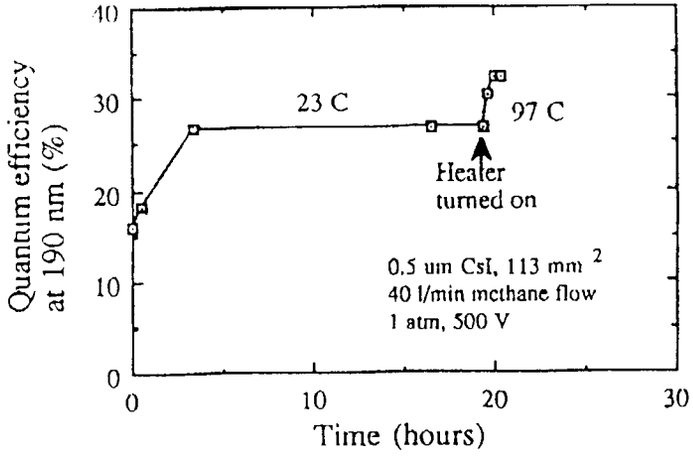

Fig. 6

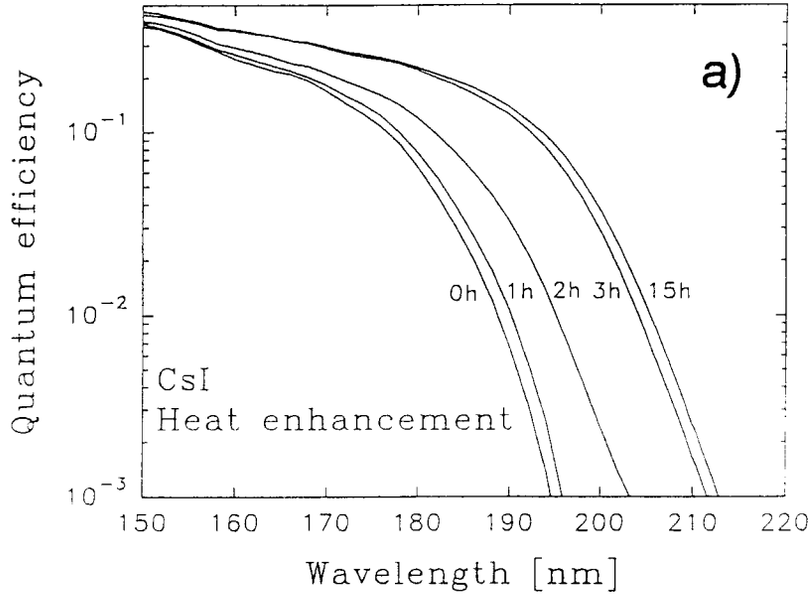

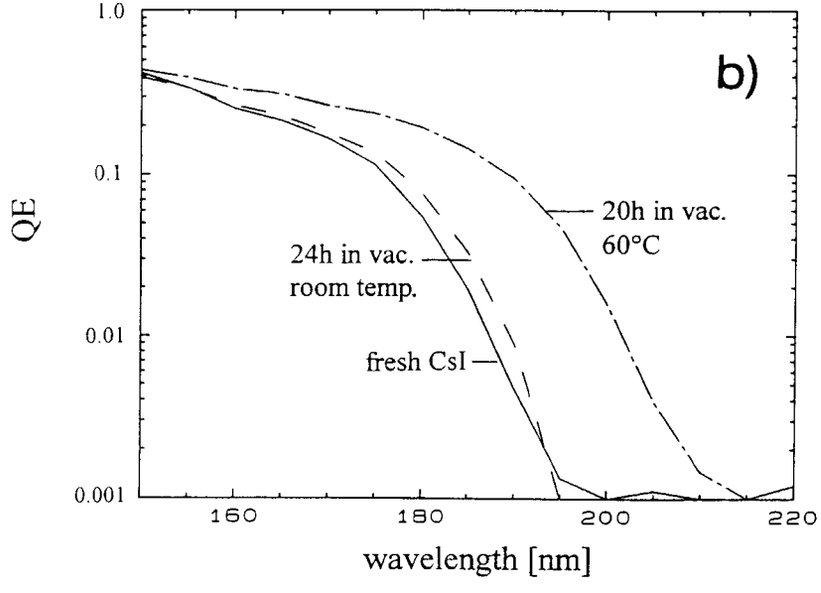

Fig. 7

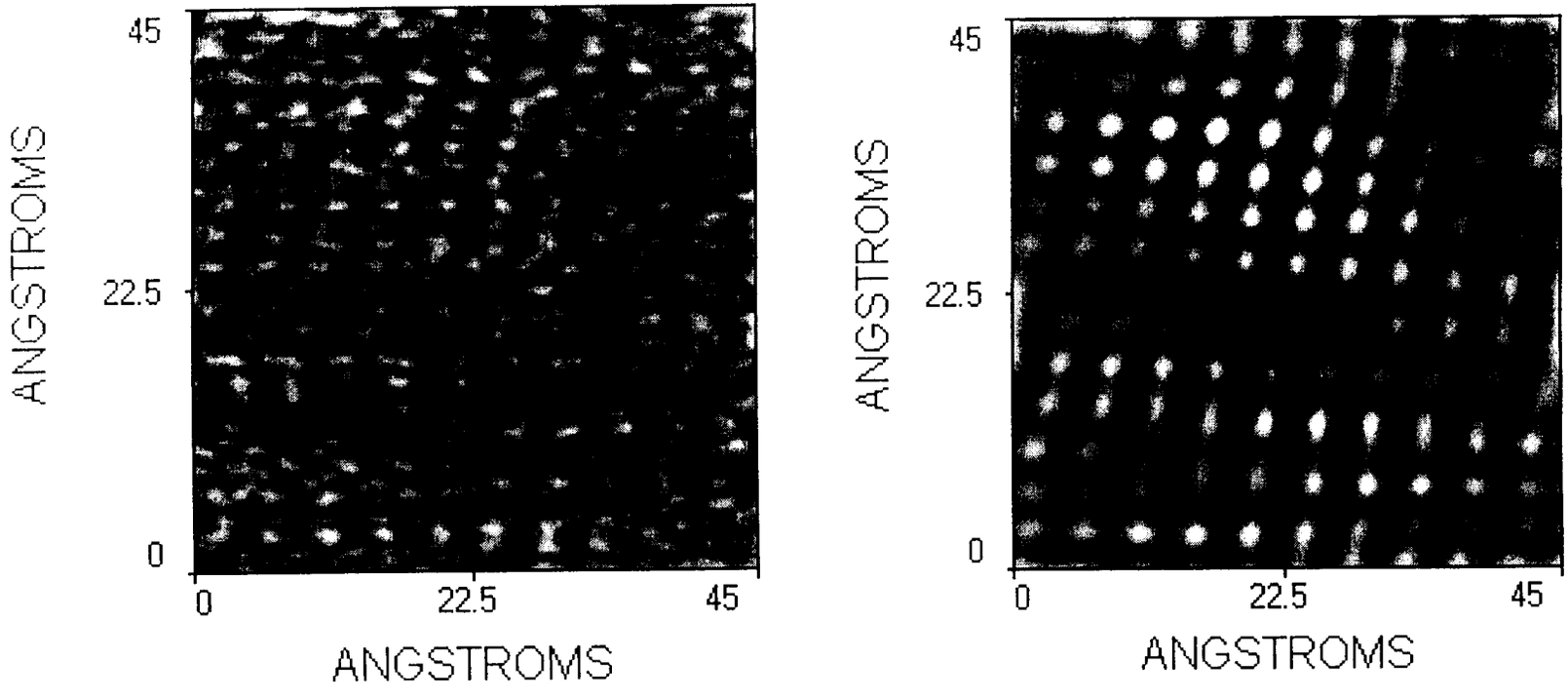
45
22.5
0
ANGSTROMS
0
22.5
45
ANGSTROMS
45
22.5
0
ANGSTROMS
0
22.5
45
ANGSTROMS

Fig. 8

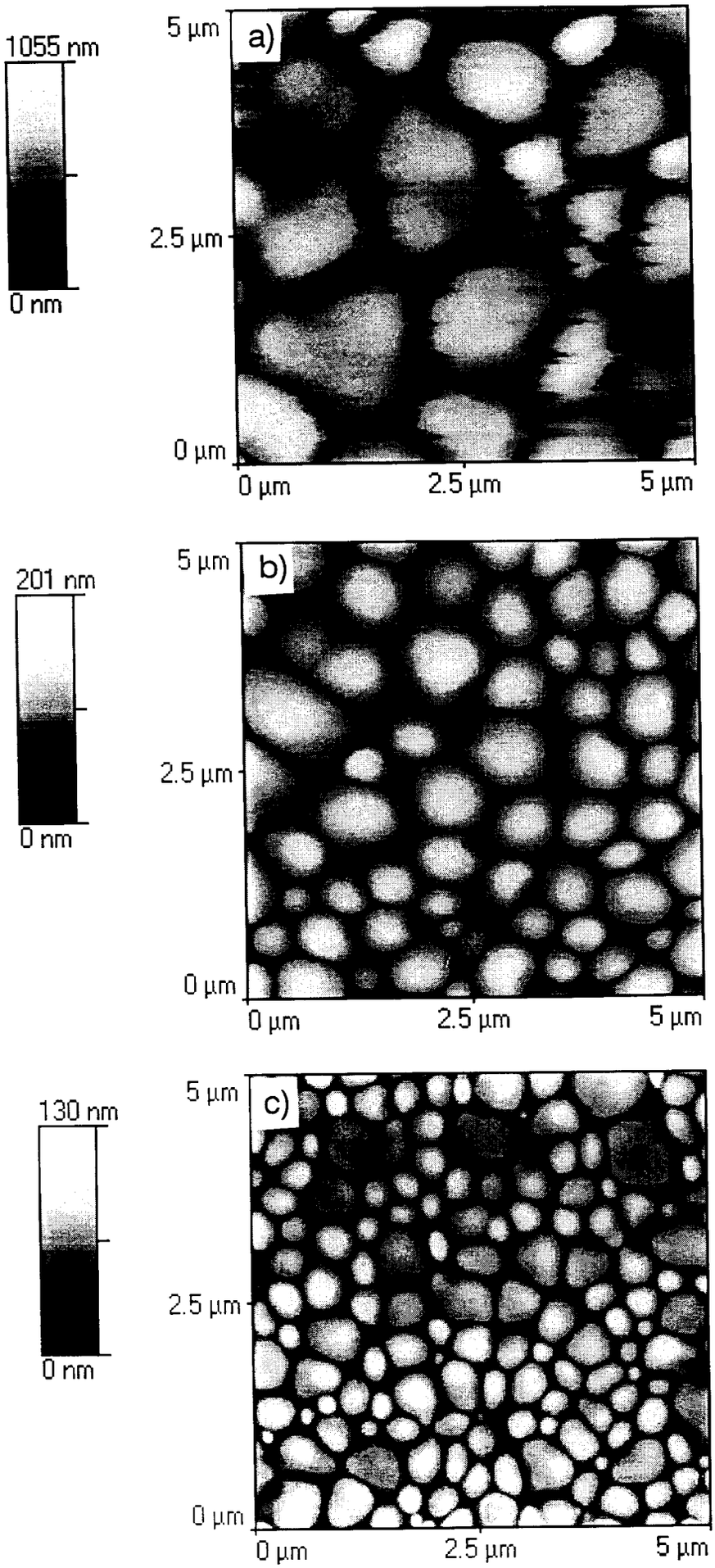
1055 nm
0 nm
5 µm
a)
2.5 µm
0 µm
0 µm
2.5 µm
5 µm
201 nm
0 nm
5 µm
b)
2.5 µm
0 µm
0 µm
2.5 µm
5 µm
130 nm
0 nm
5 µm
c)
2.5 µm
0 µm
0 µm
2.5 µm
5 µm

Fig. 9

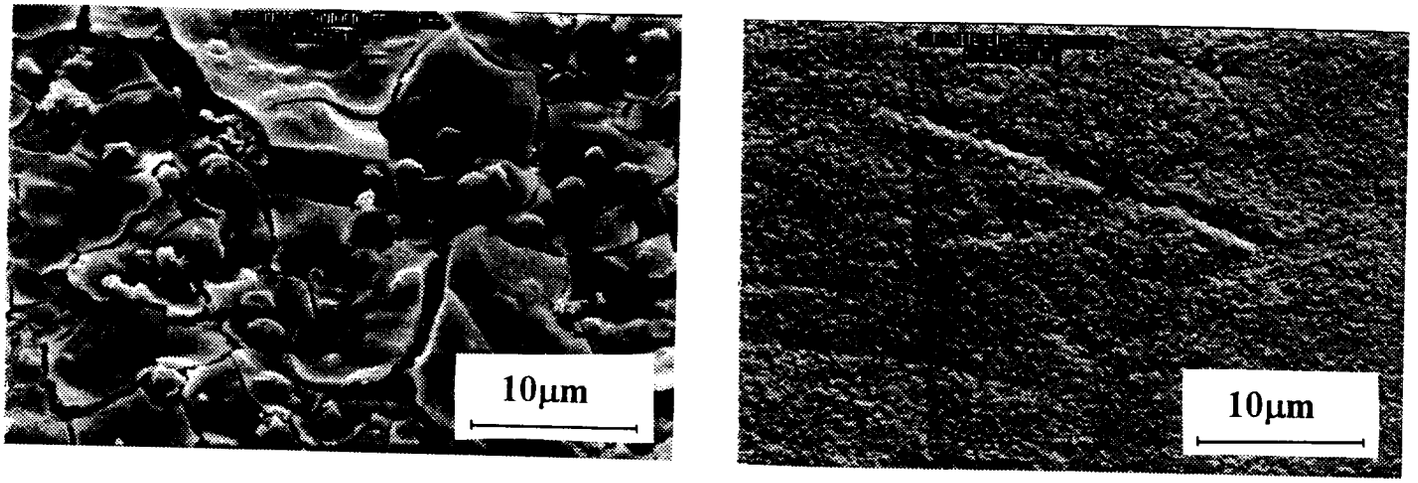
10μm
10μm

Fig. 10

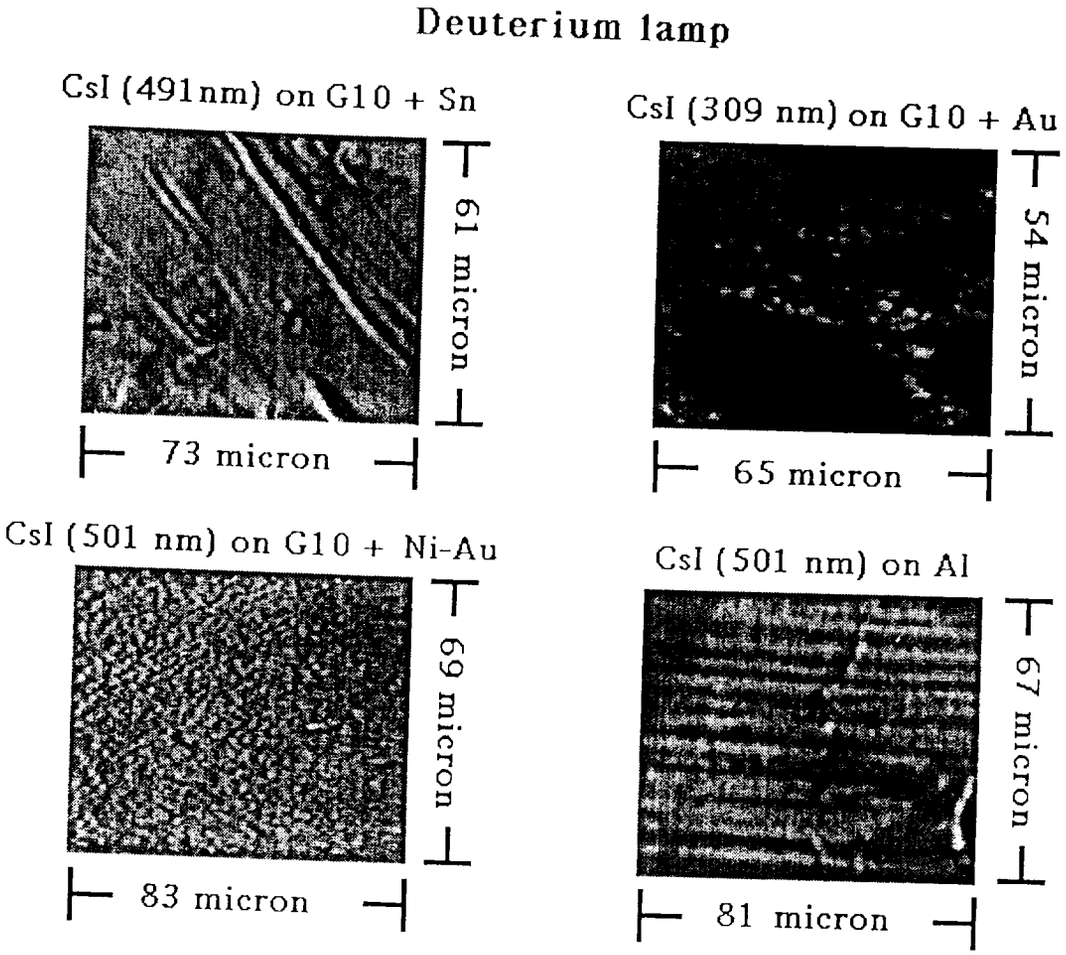
Deuterium lamp
CsI (491nm) on G10 + Sn
61 micron
73 micron
CsI (309 nm) on G10 + Au
54 micron
65 micron
CsI (501 nm) on G10 + Ni-Au
69 micron
83 micron
CsI (501 nm) on Al
67 micron
81 micron

Fig. 11

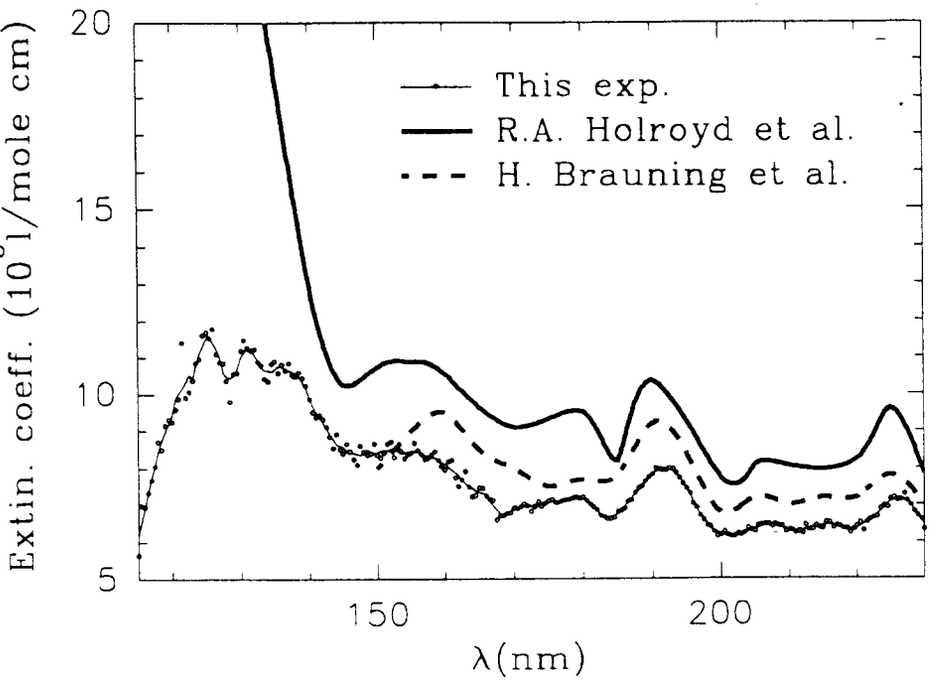
20
15
10
5
Extin. coeff. (10^3 l/mole cm)
This exp.
R.A. Holroyd et al.
H. Brauning et al.
150
200
λ(nm)

Fig. 12

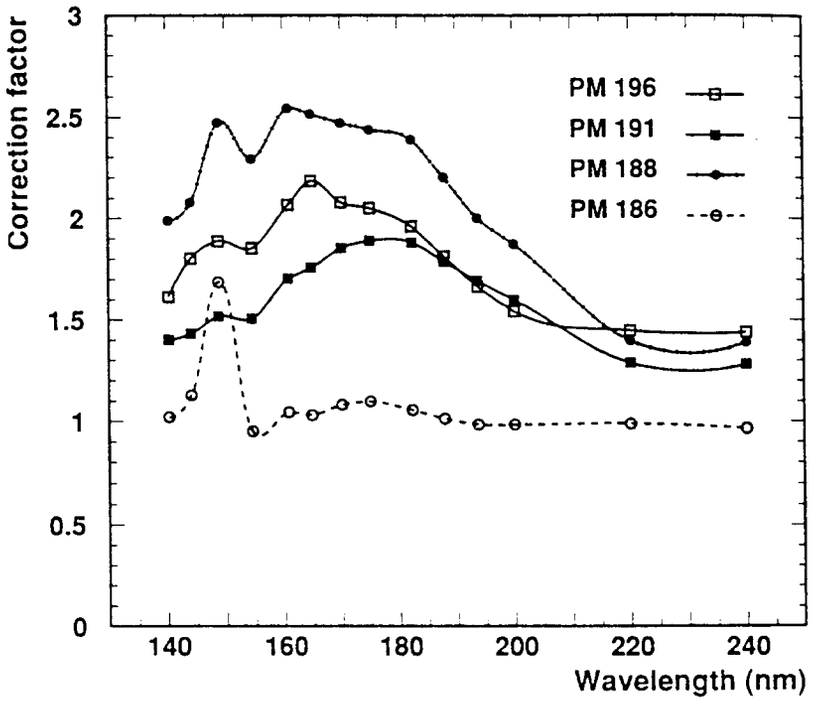
3
2.5
2
1.5
1
0.5
0
Correction factor
PM 196
PM 191
PM 188
PM 186
140
160
180
200
220
240
Wavelength (nm)

Fig. 13

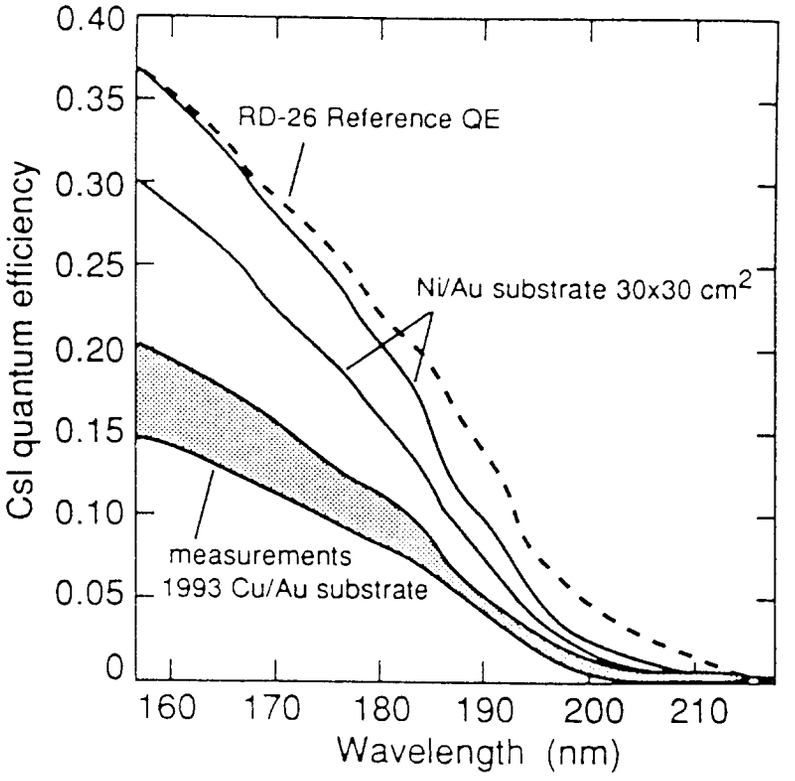
0.40
0.35
0.30
0.25
0.20
0.15
0.10
0.05
0
CsI quantum efficiency
RD-26 Reference QE
Ni/Au substrate 30x30 cm2
measurements
1993 Cu/Au substrate
160
170
180
190
200
210
Wavelength (nm)

Fig. 14

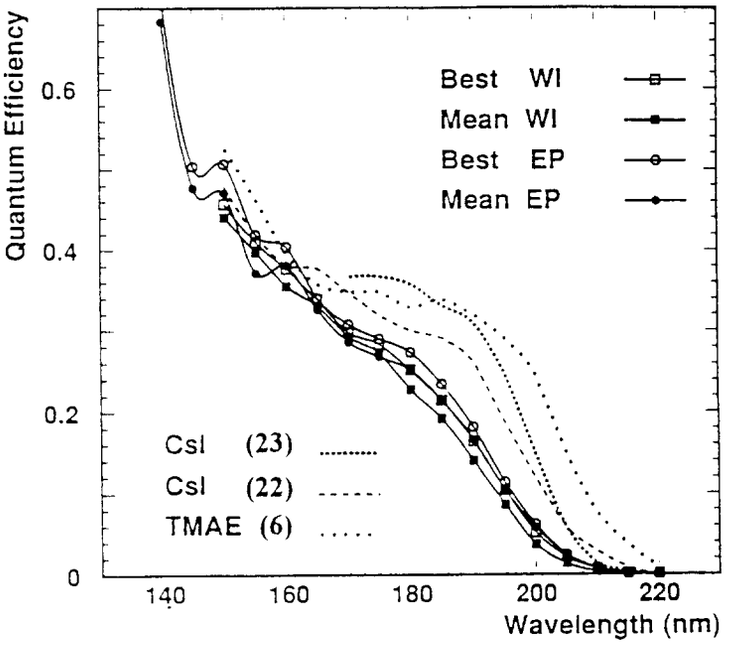
Quantum Efficiency
0.6
0.4
0.2
0
Best WI
Mean WI
Best EP
Mean EP
CsI (23)
CsI (22)
TMAE (6)
140
160
180
200
220
Wavelength (nm)

Fig. 15

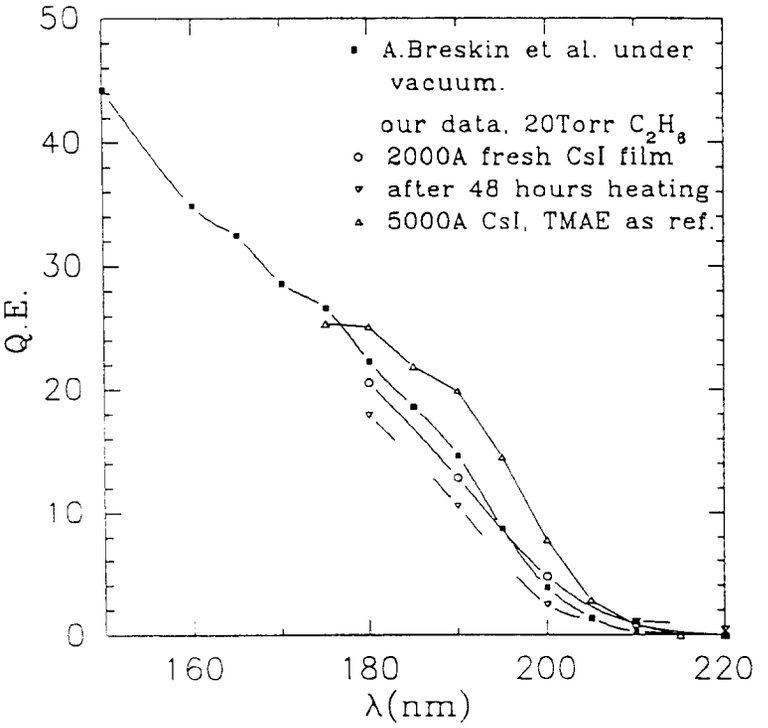
A.Breskin et al. under vacuum.
our data, 20Torr C_2H_6
2000A fresh CsI film
after 48 hours heating
5000A CsI, TMAE as ref.
Q.E.
λ(nm)
0
10
20
30
40
50
160
180
200
220

Fig. 16

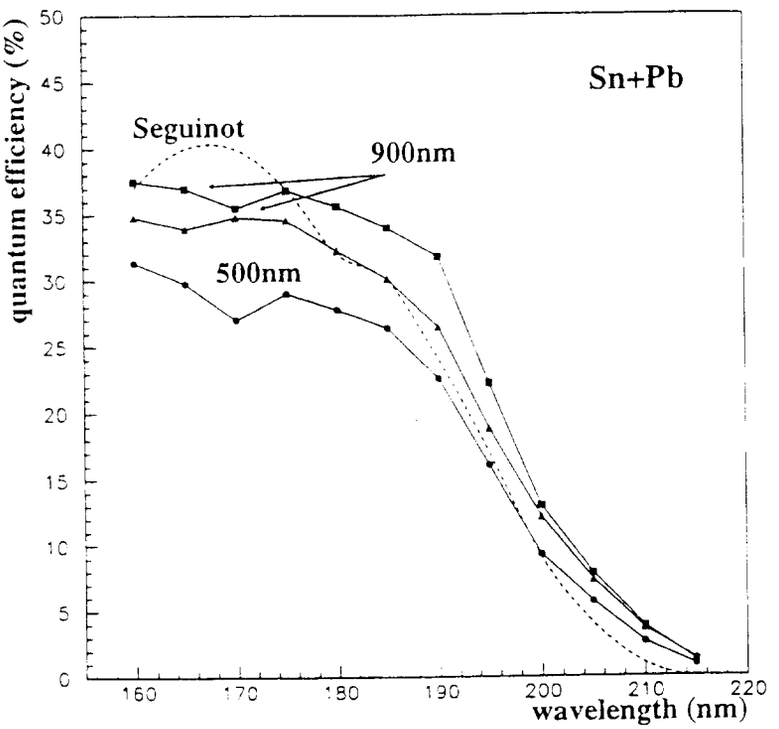
Sn+Pb
Seguinot
900nm
500nm
quantum efficiency (%)
wavelength (nm)
0
5
10
15
20
25
30
35
40
45
50
160
170
180
190
200
210
220

Fig. 17

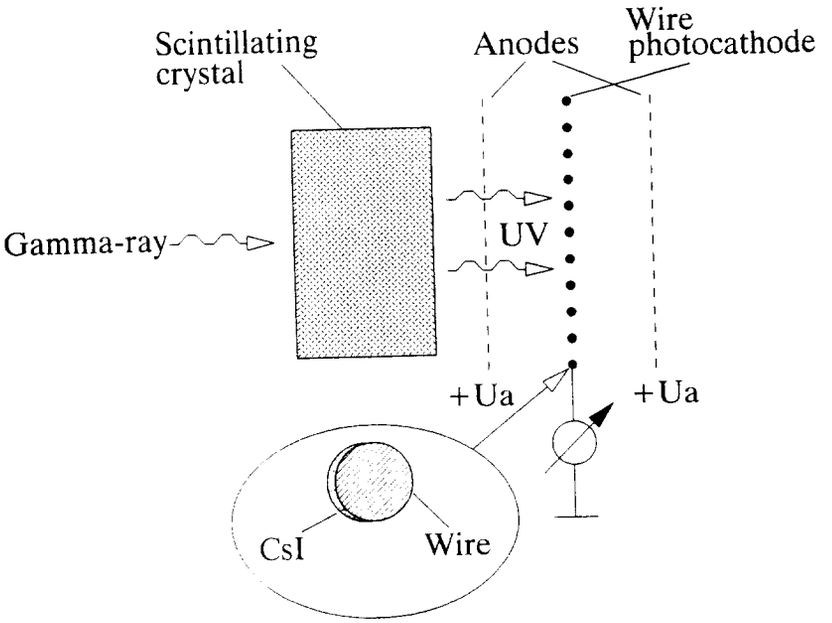
Scintillating crystal
Anodes
Wire photocathode
Gamma-ray
UV
+Ua
+Ua
CsI
Wire

Fig. 18

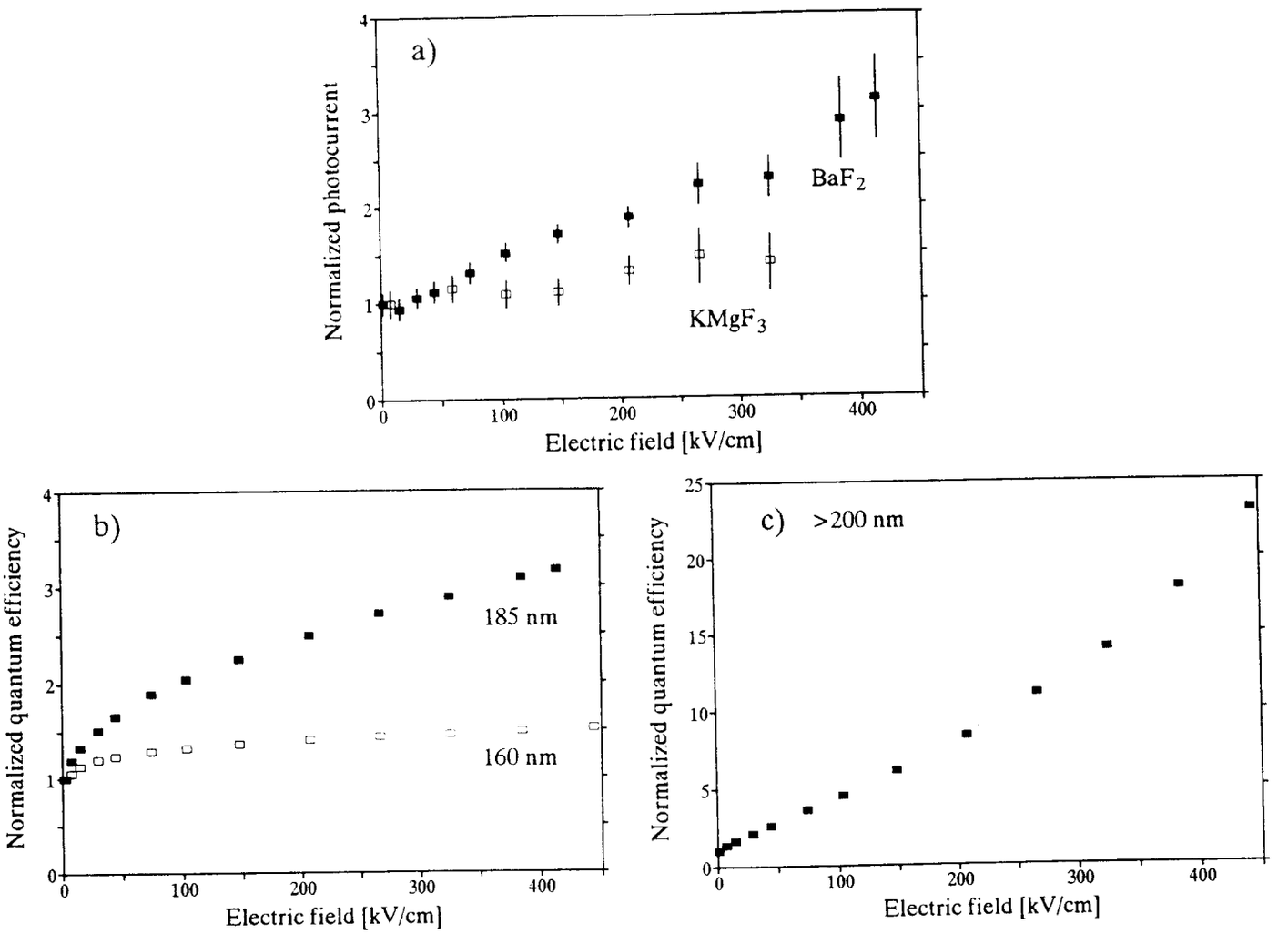
a)
Normalized photocurrent
BaF2
KMgF3
Electric field [kV/cm]
b)
Normalized quantum efficiency
185 nm
160 nm
Electric field [kV/cm]
c) >200 nm
Normalized quantum efficiency
Electric field [kV/cm]

Fig. 19

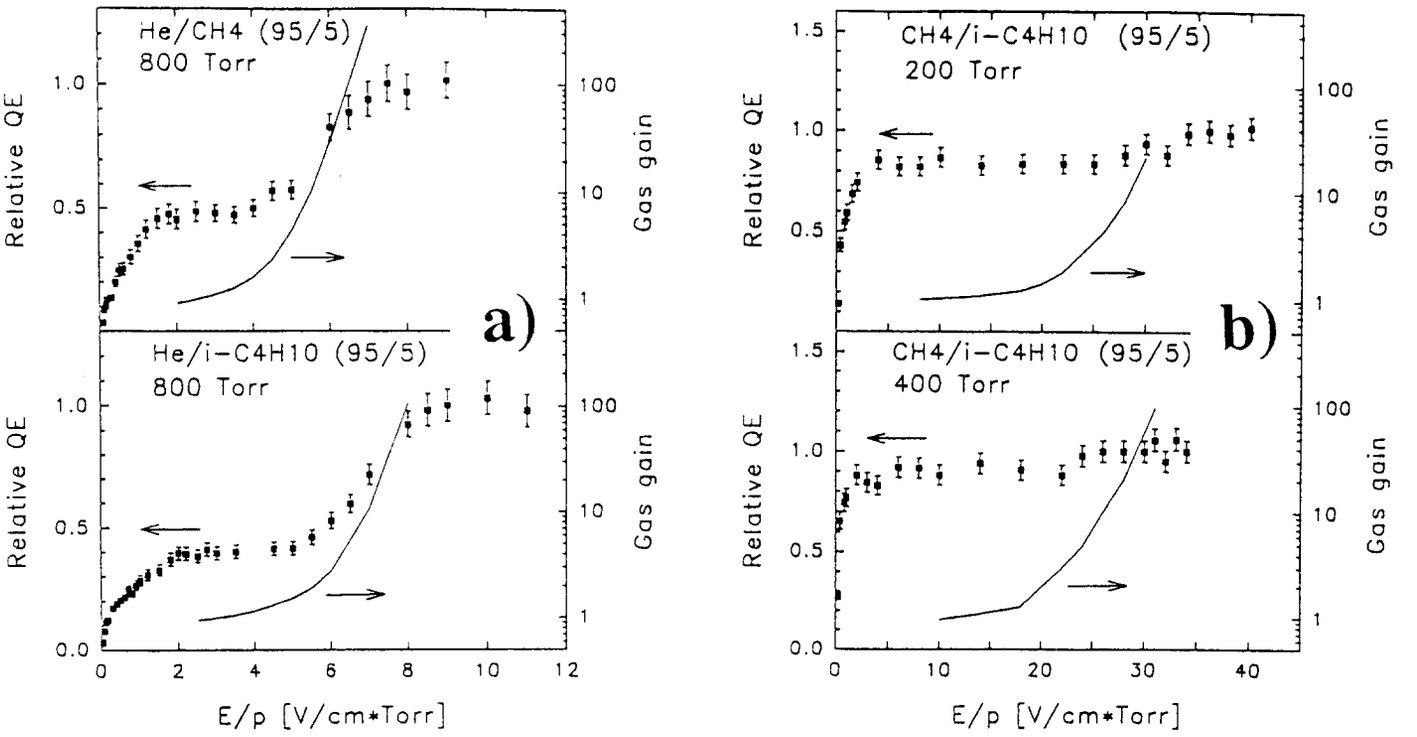
He/CH4 (95/5)
800 Torr
a)
He/i-C4H10 (95/5)
800 Torr
CH4/i-C4H10 (95/5)
200 Torr
b)
CH4/i-C4H10 (95/5)
400 Torr
Relative QE
Gas gain
E/p [V/cm*Torr]

Fig. 20

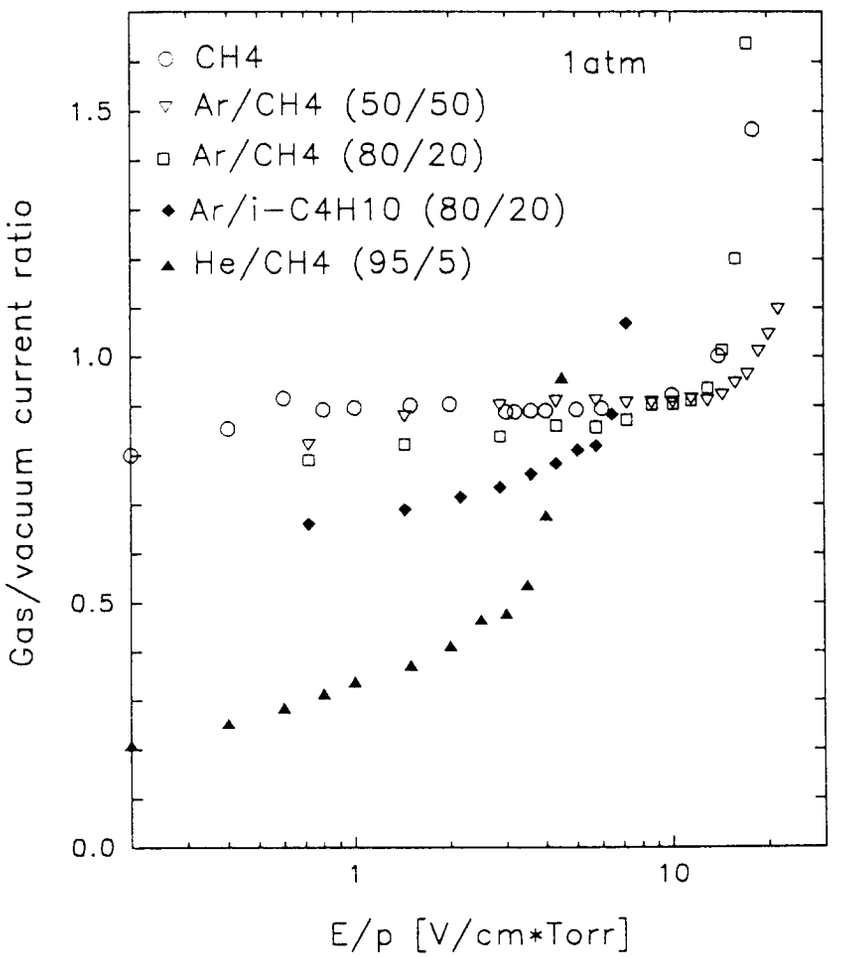
CH4
Ar/CH4 (50/50)
Ar/CH4 (80/20)
Ar/i-C4H10 (80/20)
He/CH4 (95/5)
1atm
Gas/vacuum current ratio
E/p [V/cm*Torr]

Fig. 21

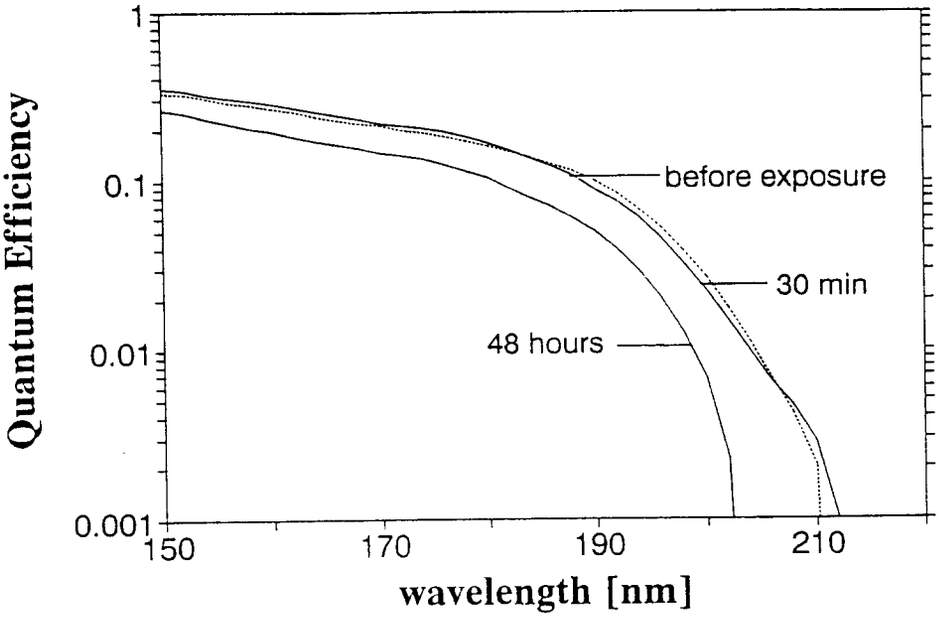
Quantum Efficiency
1
0.1
0.01
0.001
150
170
190
210
wavelength [nm]
before exposure
30 min
48 hours

Fig. 22

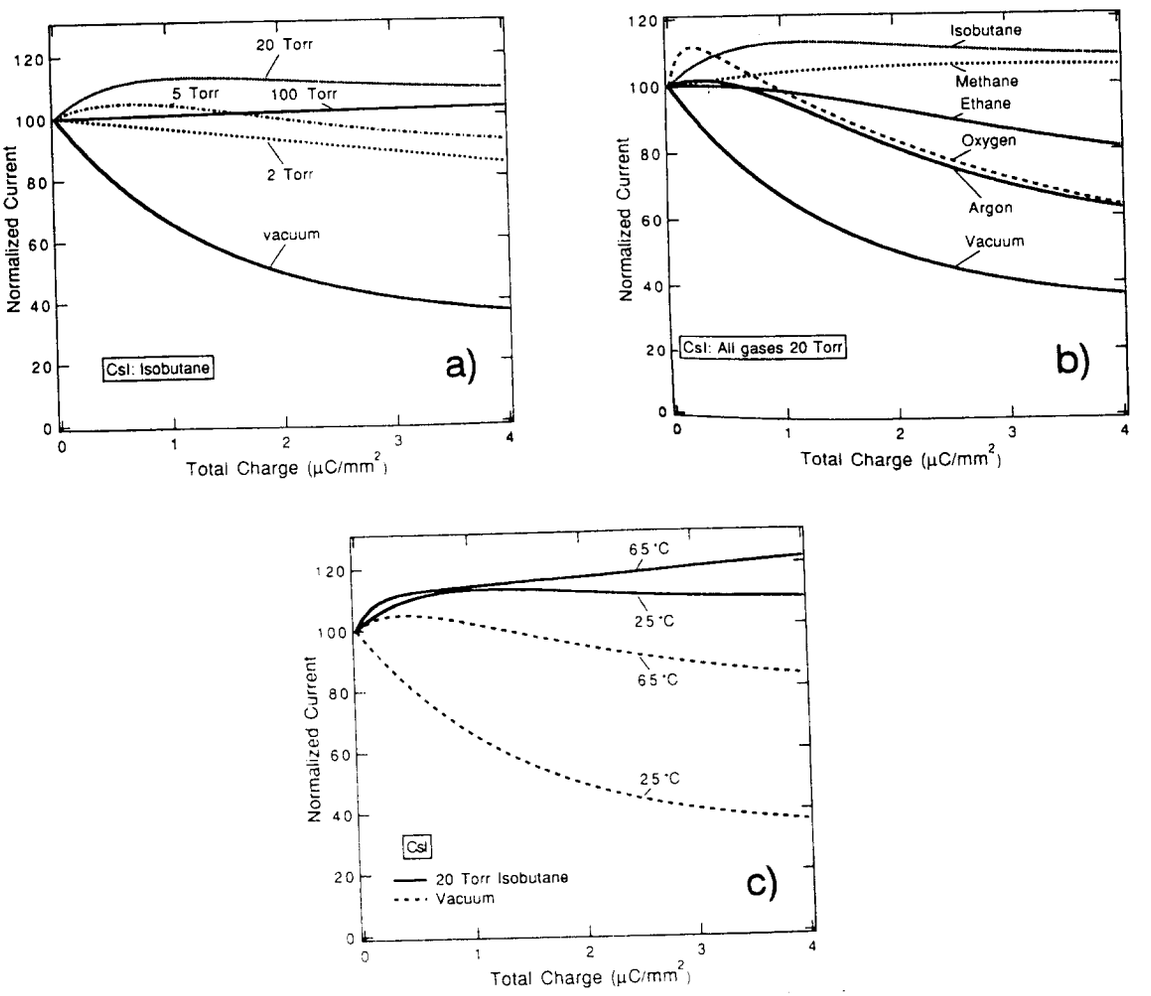
Normalized Current
Total Charge (μC/mm²)
20 Torr
5 Torr
100 Torr
2 Torr
vacuum
CsI: Isobutane
a)
Isobutane
Methane
Ethane
Oxygen
Argon
Vacuum
CsI: All gases 20 Torr
b)
65 °C
25 °C
65 °C
25 °C
CsI
20 Torr Isobutane
Vacuum
c)

Fig. 23

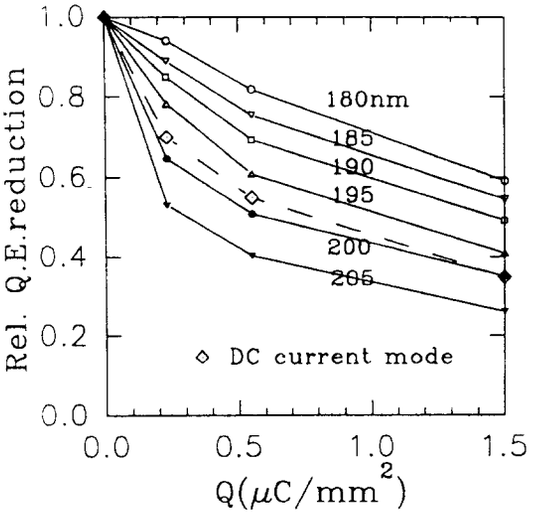

Fig. 24

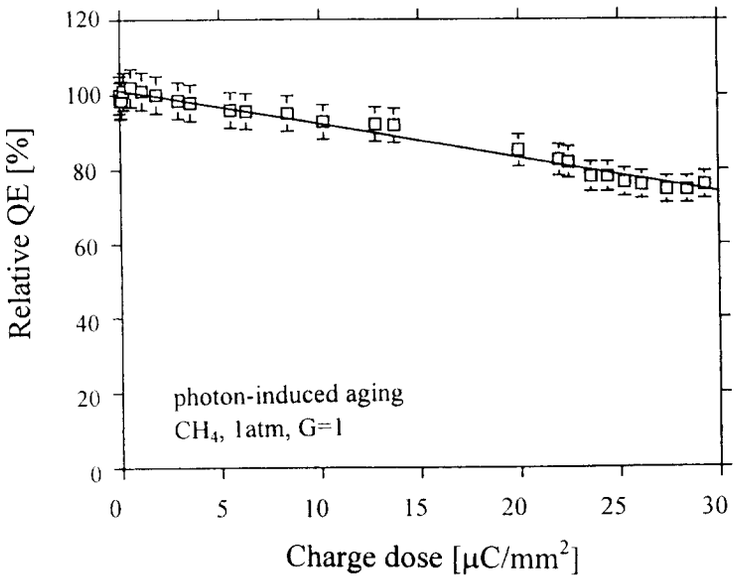

Fig. 25

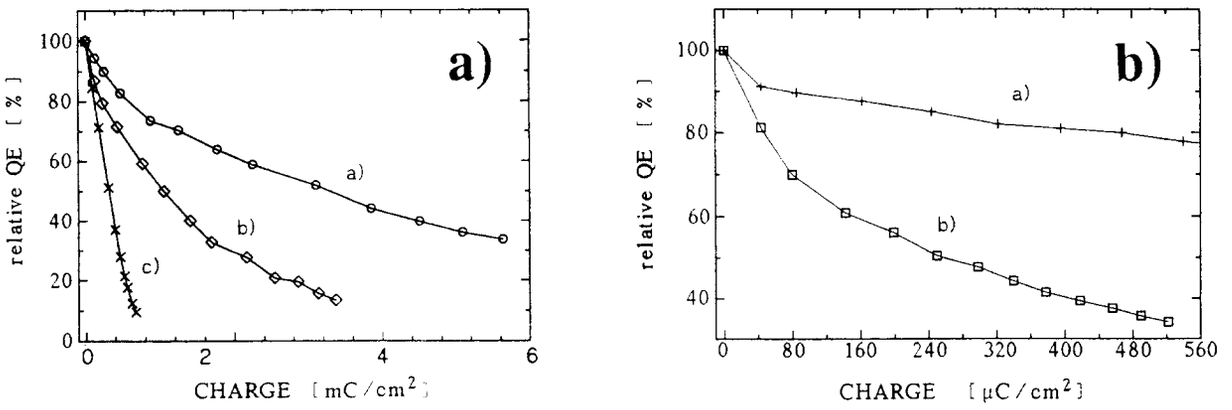

Fig. 26

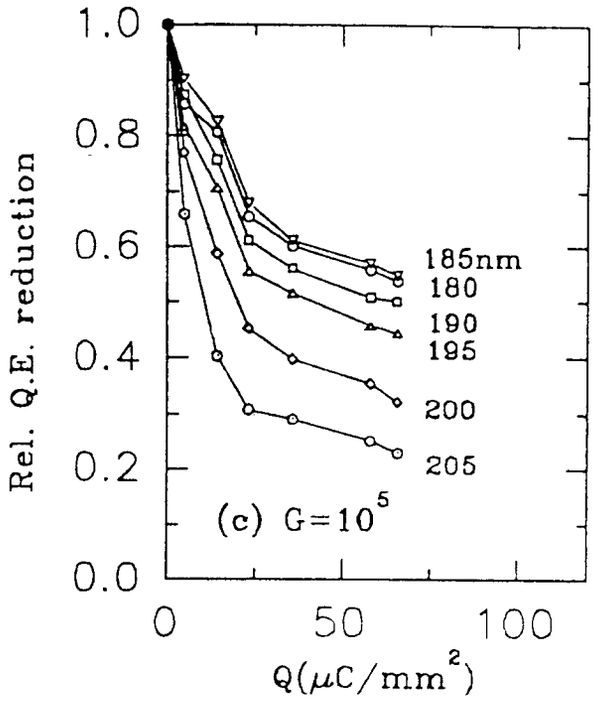

Fig. 27

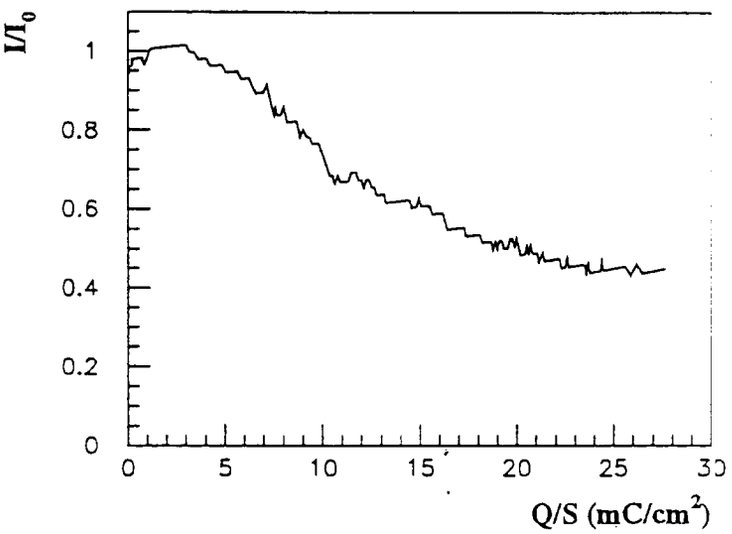

Fig. 28

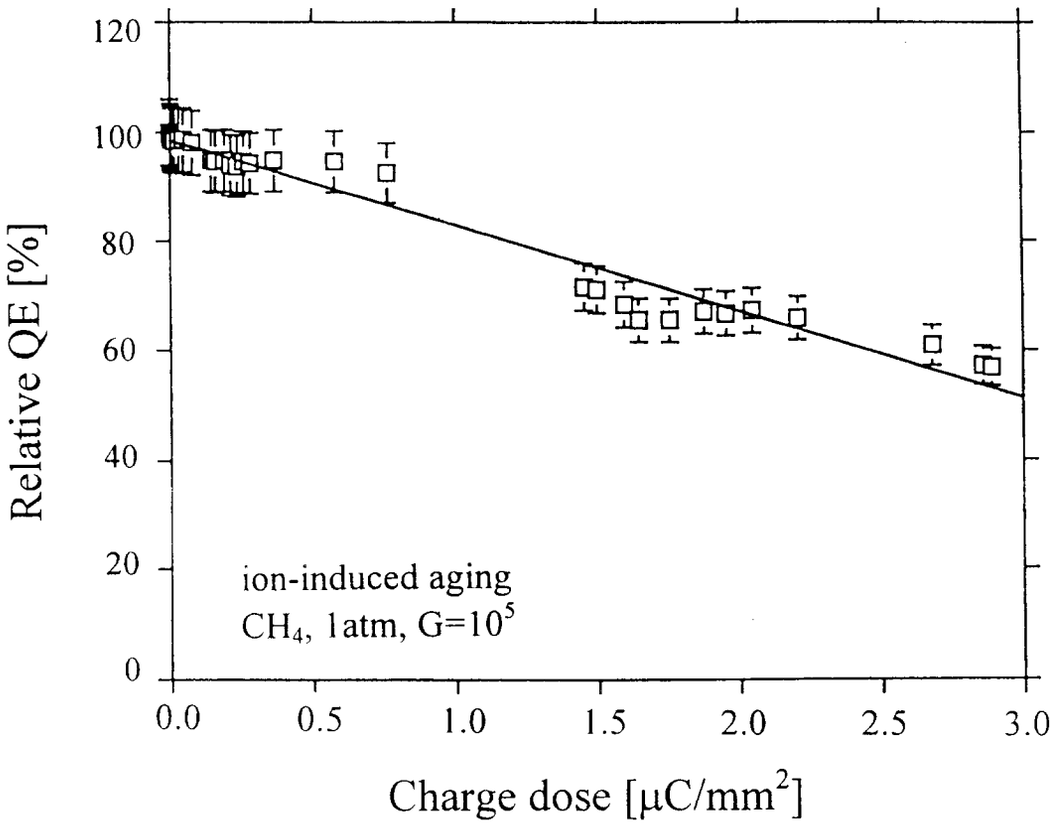

Fig. 29

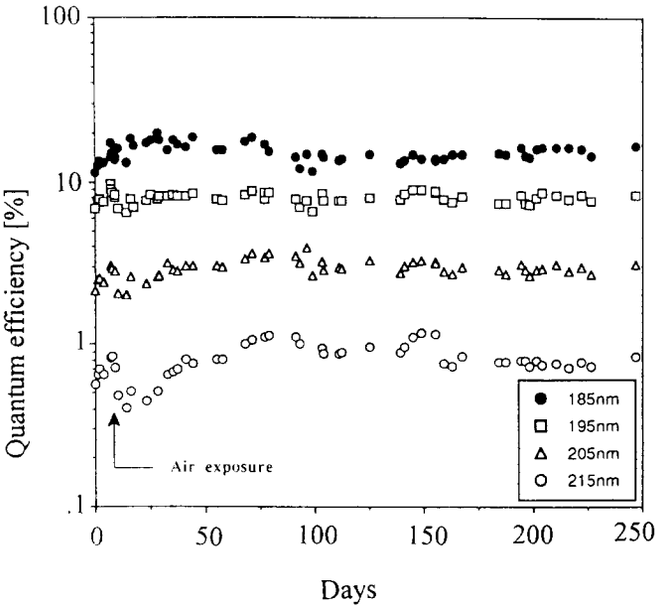
Quantum efficiency [%]
100
10
1
.1
0
50
100
150
200
250
Days
Air exposure
185nm
195nm
205nm
215nm

Fig. 30

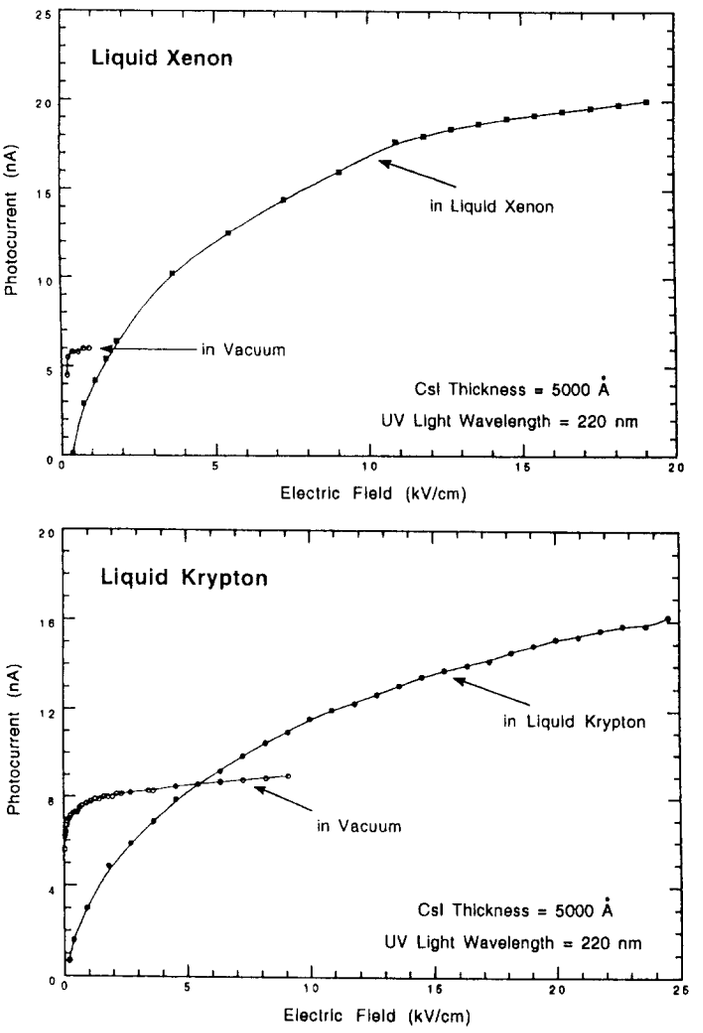
Liquid Xenon
Photocurrent (nA)
in Liquid Xenon
in Vacuum
CsI Thickness = 5000 Å
UV Light Wavelength = 220 nm
Electric Field (kV/cm)
Liquid Krypton
Photocurrent (nA)
in Liquid Krypton
in Vacuum
CsI Thickness = 5000 Å
UV Light Wavelength = 220 nm
Electric Field (kV/cm)

Fig. 31

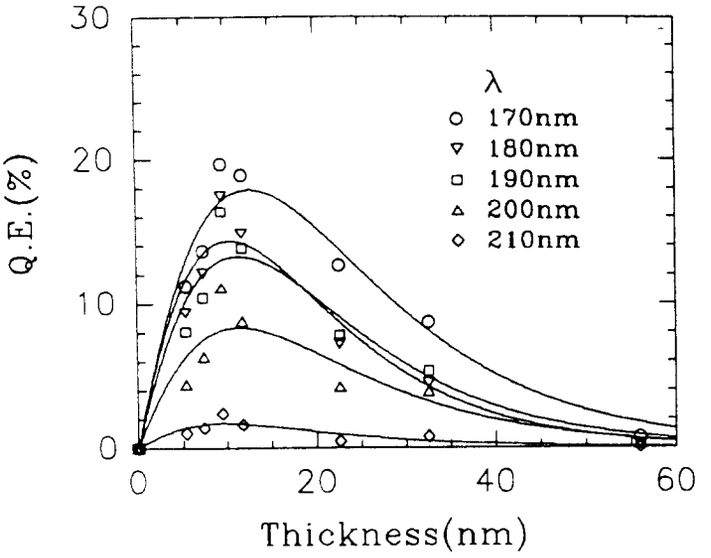

Fig. 32

a)

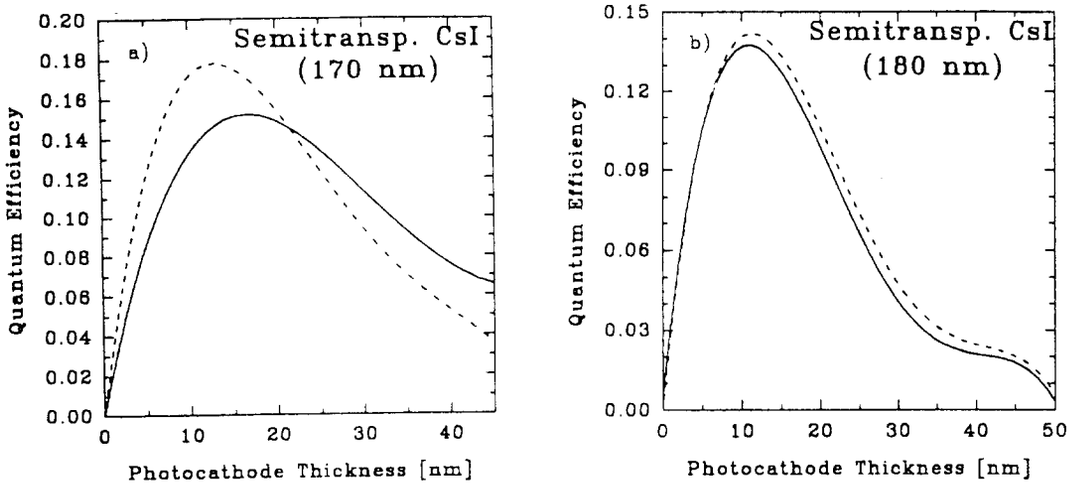

b)

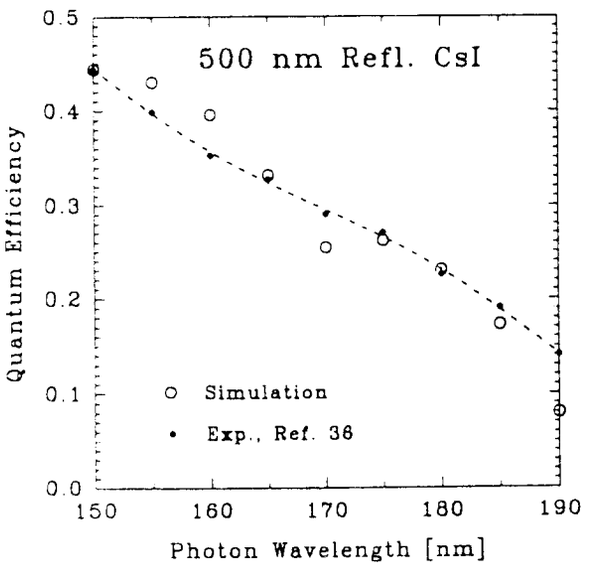

Fig. 33